Magmatism of the Devonian Altai-Sayan Rift System: Geological and geochemical evidence for diverse plume-lithosphere interactions

Alexander Vorontsov [a,b,*], Vladimir Yarmolyuk [c], Sergei Dril [a], Richard Ernst [d,e], Olga Perfilova [f], Oleg Grinev [d], Tatyana Komaritsyna [a]

[a] Institute of Geochemistry, Russian Academy of Sciences, Siberian Branch, Irkutsk, Russia
[b] Irkutsk State University, Irkutsk, Russia
[c] Institute of Geology of Ore Deposits, Petrography, Mineralogy and Geochemistry, Russian Academy of Sciences, Moscow, Russia
[d] National Research Tomsk State University, Tomsk, Russia
[e] Carleton University, 1125 Colonel By Drive, Ottawa, ON K1S 5B6, Canada
[f] Siberian Federal University, Krasnoyarsk, Russia

ARTICLE INFO

ABSTRACT

The geodynamic environment of the 407–392 Ma Altai-Sayan Rift System is characterized using previously published and new original data on whole rock, trace and Sr-Nd isotopic compositions, along with U-Pb zircon ages. Five magmatic associations are present: basalt (basalts and basaltic trachyandesites), continuous (basalts, andesites, dacite-rhyolites), alkaline (basalts, nephelinite, tephrite, phonotephrite, phonolite, teralite, ijolite-urthite, foyaite, nepheline and alkaline syenite), bimodal (trachybasalts, trachyrhyolites-pantellerites and peralkaline granites) and ultramafic-mafic (picrites and picrodolerites). Mafic rocks of basalt, continuous, alkaline, and bimodal associations exhibit a wide variation of TiO_2 (from 1.05 to 4.05 wt%) and are compositionally intermediate between intraplate basalts of OIB type and basalts of active continental margins IAB type. The TiO_2 content in these mafic rocks correlates directly with the content of large ion lithophile elements (LILE), rare-earth elements (REE), high field strength elements (HSFE), and particularly with Nb and Ta. The basaltic samples have positive $\varepsilon Nd(395)$ values ($+3.4$ to $+7.7$) and a large range of $\varepsilon Sr(395)$ values (-13.6 to $+12.6$). $\varepsilon Sr(395)$ decreases with increasing TiO_2 abundance. Pantellerites and alkaline granites have ore-level concentrations of Nb, Ta, Zr, Hf, REE; and they have similar Sr and Nd isotope parameters to those of the high-Ti basalts. This indicates their origin via fractionation of mantle magmas. Rhyolite samples are depleted in rare incompatible elements, but have low positive $\varepsilon Nd(395)$ values ($+1.5$ to $+1.8$), and $\varepsilon Sr(395)$ values ($+16.6$ to $+20.6$), and they compositionally resemble the rocks produced from anatectic magmas of crustal origin.

Whole-rock elemental and isotopic data suggest that the mafic rocks were likely derived from lithospheric mantle that was metasomatized during the prior Caledonian accretion/subduction event. In combination with the field relationship and regional geology, our study suggests that the rock associations from the Devonian Altai-Sayan Rift System were derived by the activity of mantle plumes.

1. Introduction

Continental rifting is commonly accompanied by magmatism resulting in the formation of basalt, bimodal basalt-trachyrhyolite and basalt-pantellerite associations. However, some continental rift zones also produce continuous basalt-andesite-rhyolite and andesite-rhyolite associations typifying zones of convergence. Their joint occurence makes it problematic to reconstruct geodynamic settings and plumbing systems fitting the emplacement of such geochemically different magmatic associations in a rift setting. An important example of such diverse magmatic combinations is evidenced in the Middle Paleozoic rift structures of the Altai-Sayan fold belt.

The Altai-Sayan fold belt originated through the accretion of Late Neoproterozoic-Cambrian rocks to the southwestern margin of the Siberian continent. These rocks formed within the Paleo-Asiatic Ocean as oceanic ridges and islands, island arcs and marginal basins (Zonenshain et al., 1991; Dobretsov et al., 2003; Yarmolyuk et al., 2006; Windley et al., 2007). These accretionary processes affected vast regions, and triggered formation of the Early Paleozoic (Caledonian) Altai-Sayan fold belt of the Siberian Platform (Liu et al., 2017; Wang et al., 2016; Zhao et al., 2018). Accretion started in the Late Cambrian–Early Ordovician and

completed with folding, metamorphism and orogenesis (Kröner et al., 2014, 2017; Wang et al., 2010; Xiao et al., 2010; Safonova and Santosh, 2014). This was followed by erosional exposure of granitoid batholiths (Vladimirov et al., 1999; Izokh et al., 2008; Rudnev, 2013; Rudnev et al., 2009, 2013; Jahn et al., 2000; Yarmolyuk et al., 2008, 2011b, 2014, 2016; Kruk et al., 2011; Kruk, 2015). The post-orogenic history included episodic Late Ordovician anorogenic magmatic activity in the northern Altai-Sayan region (Perfilova et al., 1999, 2004).

A new significant stage of commenced in the end of the Early Devonian (Berzin and Kungurtsev, 1996) with rifting processes beginning at 407 Ma (border between the Pragian and Emsian (Gradstein et al., 2012, 2020) in the eastern within-continent zone lying 300–600 km to the east (in present coordinates) of the paleocontinent boundary.

This is where the triple junction system (Burke and Dewey, 1973) of large linear troughs emerged, including the Deljuno-Yustyd and Tuva troughs which are connected at an angle of 100° (Figs. 1 and 2). On their margins, numerous secondary troughs and grabens originated, e.g. Minusinsk, Kansk, Agulsk, Kuznetsk Alatau and northwestern Mongolian (Yarmolyuk and Kovalenko, 1991, 2003; Yarmolyuk et al., 2000; Vorontsov et al., 1997; Gordienko, 2006; Grinev, 2007; Kuzmin et al., 2010). We have distinguished this system of grabens and troughs as the Altai-Sayan Rift System (ASRS).

The next stage of activity commenced in the Early Devonian after 395 Ma. At that time, the near-oceanic margin of the Altai-Sayan fold belt became involved in convergence processes, which resulted in an active continental margin (Polyakov et al., 1972; Kruk et al., 2008; Zonenshain et al., 1991; Jahn et al., 2000; Windley et al., 2007; Xiao et al., 2010; Kuibida et al., 2020; Sengör et al., 1993; Vladimirov et al., 2003; Rotarash et al., 1982; Scherba et al., 1998; Pirajno, 2010; Cai et al., 2011). This was due to the subduction of the Chara oceanic plate underneath the Caledonian framing of the Siberian continent and emergence of the marginal volcano-plutonic belt. During the early stage of the Emsian-Eifelian a contrasting rhyolite-

basalt association occurred, and at the later stage of Givetian-Frasnian epoch the rhyolite-basalt-rhyolite volcanism of pendulum nature took place. As regards the total volume, felsic rocks predominate over basic volcanics in the ratio of 75:25%. U-Pb SHRIMP-II ages of syngenetic granitoids revealed the first and second stages to be ~395–384 Ma (Kuibida et al., 2015) and ~ 378–372 Ma (Murzin et al., 2001), respectively.

It is noteworthy, that the Devonian margin of the Altai-Sayan fold belt was heterogeneous in trend, and some of its segments rejuvenated at different times. Different segments possibly belonged to different terranes that merged in the Early Devonian, which is indicated by their joint Early Devonian metamorphism and orogenesis (Broussolle et al., 2018). In the southern part of Chinese Altai, magmatic events are dated as 410–400 Ma in the Cambrian-Ordovician accertionary wedge (Broussolle et al., 2018). However, the geological structures of the Altai-Sayan fold belt existed as one unit by the Early-Middle Devonian within the period 395–376 Ma. At that time, subduction-related magmatism was proceeding along the margin of the Siberian continent in the Gorny Altai (Kruk et al., 2008; Xiao et al., 2010; Kuibida et al., 2020) and in the Chinese Altai (Cui et al., 2020).

Magmatism of ASRS has been explored previously. For the past three decades valuable data has been gained from the Minusinsk, Kuznetsk-Alatau and Northern Mongolian segments, as well as the Deljuno-Yustyd and Tuva troughs. Herein, we summarize some important inferences made through these earlier studies.

(1) Within ASRS, the magmatism displays heterogeneous features (Fig. 2). The basalt association was mostly widespread; it produced sequences of moderately alkaline basalts and basaltic trachyandesites. In addition, abundant bimodal associations in the ASRS include trachybasalts, trachyrhyolites-pantellerites and peralkaline granites (Kovalenko et al., 1989, 2004a; Vorontsov et al., 1997; Vorontsov and Sandimirov, 2010), as well as alkaline associations (Uvarov and Uvarova, 2008, 2009;
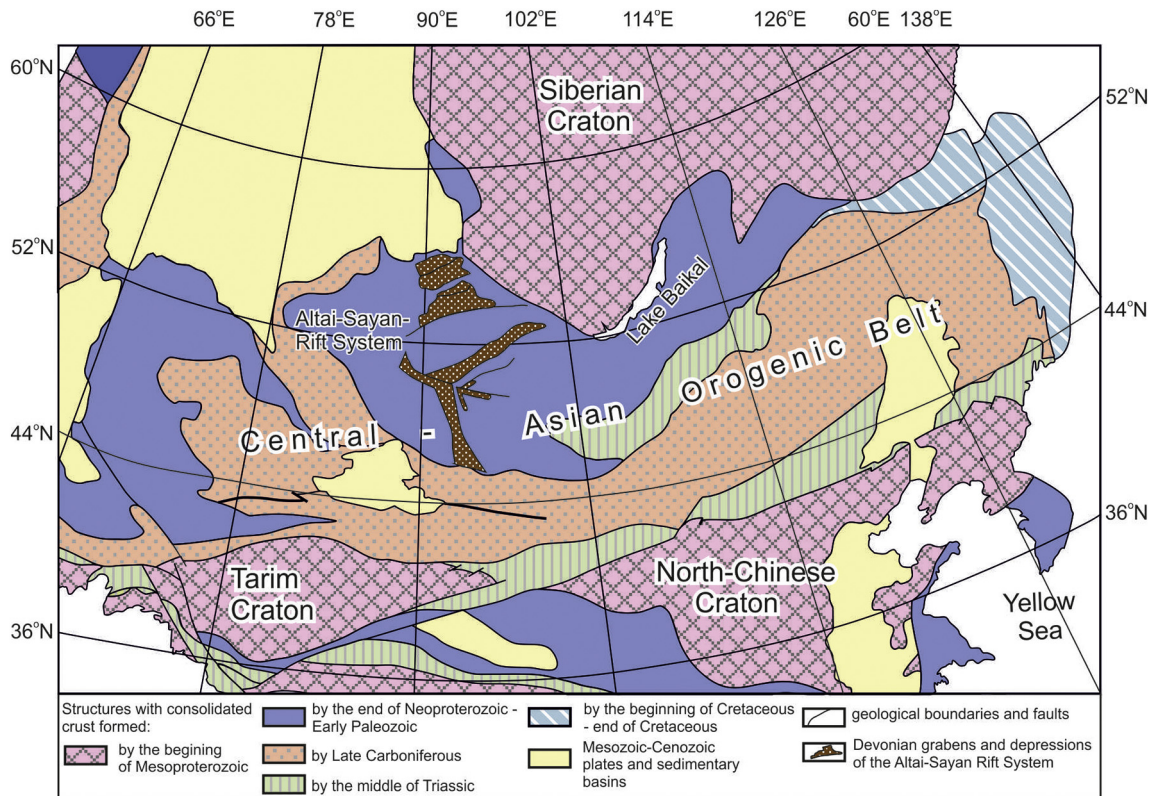

Fig. 1. Tectonic elements of Central Asia and position of Altai-Sayan Rift System within the Central Asian Orogenic Belt. Base map from Li (2008).
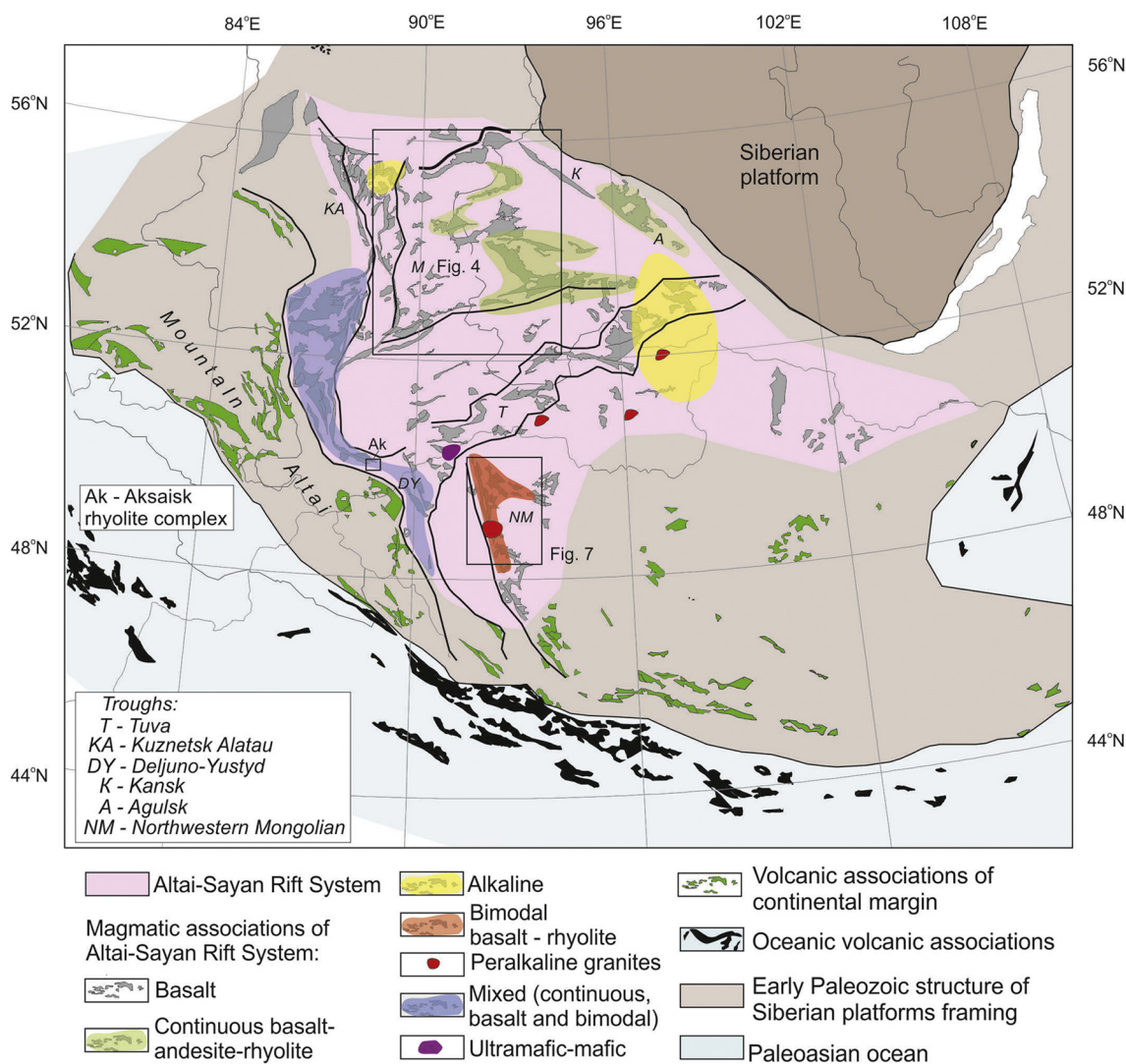
Fig. 2. Structural-tectonic map of the south-western part of the Middle Paleozoic Siberian paleocontinent (modified from Yarmolyuk et al. (2013) showing location of Devonian magmatic associations: data sources from Luchitsky (1960), Tikunov (1995), Gavrilova and Luvsandanzan (1983), Yashina (1982), Yarmolyuk and Kovalenko (1991), Yarmolyuk and Vorontsov (1993), Kovalenko et al. (2004a), Vrublevsky et al. (2016), Krupchatnikov et al. (2018), Izokh et al. (2011) . Location of Figs. 4 and 7 shown.

Grinev, 2007; Vrublevsky et al., 2016). The ultramafic-mafic association including picrite and picrodolerite developed locally (Izokh et al., 2011).

Along with these associations, which typify an intraplate setting and zones of continental rifting (Condie, 1985; Ayalew and Gibson, 2009; Dobretsov, 2011; Ernst, 2014), some additional associations were also emplaced: continuous basalt-andesite-dacite-rhyolite associations (Yarmolyuk and Kovalenko, 1991; Vorontsov et al., 2015, 2018) and those of felsic rocks (Krupchatnikov et al., 2018) of a type common for active continental margins (Miyashiro, 1974; Tatsumi and Eggins, 1995; Kelemen et al., 2003; Dobretsov, 2010).

(2) The volcanism of the ASRS is localized mainly in rift troughs and grabens rather than in the form of widespread flood basalts. Primary outlines of volcanic fields were affected by the post-Devonian tectonic events occurring widely over this territory (Luchitsky, 1960; Devyatkin, 1974; Nagibina, 1974; Yarmolyuk and Vorontsov, 1993). The magmatism of this region has many similarities to Large Igneous Provinces (LIPs) and has been termed the Altai-Sayan LIP (Kuzmin et al., 2010; Kravchinsky, 2012; Ernst et al., 2020), on the basis of the presence of triple

junction rifting indicative of a plume and the huge area about 300,000 km^2 occupied by magmatic rocks with an estimated volume about 120,000 km^3, of which at least 20,000 km^3 occur in the Minusinsk trough (Luchitsky, 1960).

(3) Geochronological Rb-Sr, K-Ar, Ar-Ar and U-Pb data available for the ASRS (Rublev and Makhlaev, 1997; Rublev et al., 1999; Malkovets et al., 2003; Lavrenchuk et al., 2004; Fedoseev et al., 2003; Fedoseev, 2008; Vrublevsky et al., 2016; Krupchatnikov et al., 2018; Vorontsov et al., 2013a; Izokh et al., 2011; Babin et al., 2004; Kovalenko et al., 2004a; Zubkov et al., 1986) indicate a range of magmatic activity from 430 to 360 Ma (Fig. 3). However, the validity of some Rb-Sr and Ar-Ar determinations seems doubtful, because some these isotope systems were disturbed. A narrower interval (407–392 Ma – Early-Middle Devonian) for the magmatic activity is confirmed based on U-Pb dating and the statistical peak on the age histograms.

As was reported above, soon after the ASRS was accreted, in the western Altai-Sayan fold belt an active continental margin (ACM) started forming along the margin of the continent with the Paleo-Asian Ocean. While an independent origin of these two events (ASRS
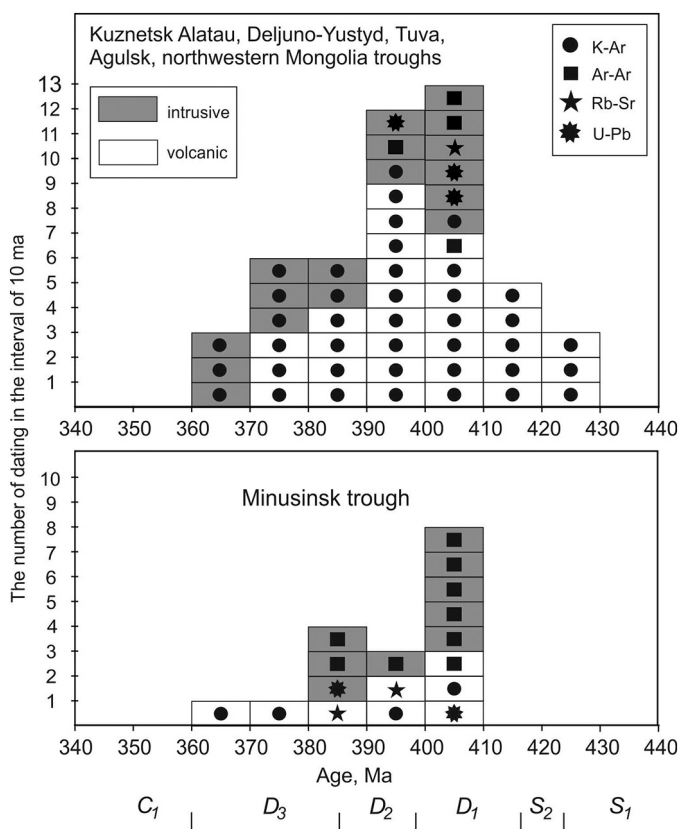
Fig. 3. Pattern of K-Ar, Ar-Ar, Rb-Sr and U-Pb dates of rocks of magmatic associations of Altai-Sayan Rift System: data sources from Rublev and Makhlaev (1997), Rublev et al. (1999), Malkovets et al. (2003), Lavrenchuk et al. (2004), Fedoseev et al. (2003), Fedoseev (2008), Vrublevsky et al. (2016), Krupchatnikov et al. (2018), Vorontsov et al. (2013a), Izokh et al. (2011), Babin et al. (2004), Kovalenko et al. (2004a), Zubkov et al. (1986).

and ACM) is possible, the match in timing suggests a genetic link. In this study, we have investigated the emplacement of these different associations within the ASRS context, and provided new geochemical and Sr-Nd isotope data to characterize rocks of these associations. Based on these new data, integrated with the preexisting data, we propose a model to explain how magmatic associations with diverse geochemical signatures, originated in the ASRS.

2. Emplacement of magmatic associations within ASRS

2.1. Basalt association

The basalt association includes moderately alkaline basalts and basaltic trachyandesites, swarms of mafic sills and dykes. The basalts dominate among the other products of magmatism and make up a significant part of thick (up to 2500 m) sedimentary volcanic sequences in all segments of ASRS (gray areas in Fig. 2). Thus, in the Minusinsk trough, the largest rift in the system, igneous rocks of these sequences are spread over an area about 100,000 km² (Luchitsky, 1960); they are referred to the Byskarsky series of Early-Middle Devonian time (Belyakov et al., 1955; Theodorovich and Polonskaya, 1958; Ohapkin, 1961; Luchitsky, 1960; Ananiev, 1959; Krasnov and Ratanov, 1974; Zakharova and Ananiev, 1990; Schneider and Zubkus, 1962; Sennikov et al., 1995; Kosorukov and Parnachev, 1994; Parnachev et al., 1996; Parnachev, 2006; Fedoseev, 2008; Khomichev et al., 2001). Volcanics crop out in the Minusinsk trough framing and in the anticlinal folds, i.e. outcrops within the trough. In its different segments the 407–392 Ma age (mentioned above) of the volcanics is consistent

with the propteridophyte flora samples found in sedimentary layers. The volcanics are discordantly overlain by faunally-dated Middle-Late Devonian (post-Zhivetian), Carboniferous-Permian and Jurassic sediments. The rocks of the Byskarsk series and its analogs discordantly overlie the Vendian-Cambrian, and Cambrian-Ordovician sequences and occur in the northwestern side of the Kansk trough in the Chernaya Sopka association (Lavrenchuk et al., 2004), in the Tuva (Vorontsov and Sandimirov, 2010; Kuznetsov, 1966; Sugorakova et al., 2009) and Agulsk troughs (Nozhkin and Smagin, 1979; Rublev et al., 1994), in the near-fault depressions of the Agardaksk belt of northwestern Mongolia (Vorontsov, 1993; Yarmolyuk and Vorontsov, 1993) and in the Kuznetsk Alatau stuctures (Markov, 1987; Grinev, 2007).

2.2. Continuous association

Rocks of the continuous series, basalt-andesite-trachyte-trachydacite-rhyolite associations, locally occur on the eastern side of the Minusinsk trough in the Batenevsk area (Vorontsov et al., 2015), in the Sisimsk volcanic field and in the Agulsk trough (Nozhkin and Smagin, 1979; Rublev et al., 1994) producing sizable lava fields up to some tens of thousands km² (dirty green areas in Fig. 2). The volcano-plutonic areas of the Deljuno-Yustyd trough are linked to the same association, which might be exemplified by the Aksaisk complex in the area southeast of the Gorny Altai (Ak in Fig. 2). The Aksaisk complex comprises andesites, dacites, rhyolites and leucogranites dated as 402–405 Ma (Krupchatnikov et al., 2018). In the west, similar magmatic associations compose part of the marginal belt of ACM; they started forming at about 395 Ma (Rudnev et al., 2001). They are widespread within the Gorny Altai (Shokalsky et al., 2000) and show geochemical signatures typical for igneous rocks of supra-subduction settings (Tikunov, 1995).

2.3. Alkaline association

The ASRS encompasses at least two provinces of Early-Middle Devonian alkaline magmatism (yellow areas in Fig. 2).

One of them is situated in northeast Kuznetsk Alatau, on the northwestern side of the Minusinsk trough. Volcanics of this province contain basalts, nephelinites, tephrites, phonotephrites and phonolites, and make up the Goryachegorsk Plateau and adjacent areas (Markov, 1987; Uvarov and Uvarova, 2008; Vorontsov et al., 2013b; Grinev et al., 2019). These units extend over 4800 km², with a volume of volcanic products is estimated as 12,000 km³. Intrusive rocks are also present and consist of small (about 2 km²) bodies of alkaline mafic rocks present in varying proportions consisting of moderately alkaline and alkaline gabbro, teralite, ijolite-urthite, foyaite, nepheline and alkaline syenite (Grinev, 1990; Makarenko and Kortusov, 1991; Vrublevsky et al., 2016). The U-Pb age of these rocks varies within 410–385 Ma. These intrusions occur in the western Early Caledonian frame of the Minusinsk trough and their emplacement is controlled by the system of Kuznetsk-Alatau deep-seated faults.

The other alkaline province lies in the eastern ASRS, e.g. within the Precambrian Tuva-Mongol microcontinent and consists of intrusions (~ 1–10 km²) located in the highlands of the East Tuva, Sangilen and western Khubsugul Lake areas and composed of alkaline gabbro, teralite, ijolite-urtite and foyaite (Yashina, 1982). The intrusive complexes are aligned along deep faults, e.g. South Minusinsk, East Sayan, Central Sangilen and Beltesingol (Northern Mongolia).

2.4. Bimodal association

Rocks of bimodal association (red area in Fig. 2) occur in northwestern Mongolia on the eastern slopes of the Mongolian Altai (Vorontsov, 1993; Yarmolyuk and Vorontsov, 1993). This is where volcanics jointly with sedimentary complexes occur in grabens controlled by large faults of the Early Caledonian Lake Zone. Grabens make up linear belts, e.g.

Khan-Khukhey and western Tsagan-Shibetinsky, extending for about 420 km. The Early Devonian age of volcanics is indicated by the fauna and flora in sedimentary rocks (Gavrilova and Luvsandanzan, 1983; Yarmolyuk and Kovalenko, 1991). The intrusive analogs of volcanics are the peralkaline-granite massifs discovered within Mongolian Altai and southern margin of the Tuva trough. Of these massifs, the Khaldzan Buregte group is the most comprehensively studied. Located close to the Kharaus-Nur lake they are hosted by the NW-striking large fault separating the Early Caledonian Lake Zone from Late Caledonides of Mongolian Altai. The U-Pb zircon age of the intrusion rocks is 395–392 Ma (Kovalenko et al., 1989, 2004a).

2.5. Ultramafic-mafic association

Ultramafic-mafic magmatism being the indicator of high melting temperatures took place in northwestern Mongolia, north of the Ureg-Nur Lake, on the eastern slopes of Tsagan-Shibetu Range (Izokh et al., 2011). This magmatism is concentrated within about 50 km of the triple junction of the Deljuno-Yustyd and Tuva troughs (purple area in Fig. 2). The ultramafic-mafic association includes picrites and picrodolerites of minor intrusions cutting the Lower Devonian volcanic sediments. Ar-Ar and U-Pb ages of the rocks span the interval 406–391 Ma. The volume of these mafic-ultramafic rocks is minor in comparison with the other types of rocks and associations.

3. Geological characteristics

The different magmatic groups of the ASRS are best displayed in the following regions:

(a) Basalt association in the Kopjevsk and Novosjelovsk areas.
(b) Continuous volcanic association in the Batenevsk area.

(c) Alkaline volcanic association on Goryachegorsk plateau.
(d) Bimodal volcano-plutonic association in the Lake Zone grabens in northwestern Mongolia.

3.1. Basalt association of the Kopjevsk and Novosjelovsk area

The Kopjevsk and Novosjelovsk areas host fragments of the Devonian volcanic plateau of the Minusinsk trough.

The Kopjevsk area sits in the center of Minusinsk trough in upstream portions of the Chulym River (Fig. 4 and 5a) covering an area of 1,000 km². It looks like an isometric anticline structure, with its domal part and flanks composed of Devonian sediments and volcanics of the Byskarsk series that are about 1,500 m thick. The series overlies with angular unconformity the Cambrian-Ordovician basement that hosts altered effusive rocks and sedimentary-metamorphic formations (Kosorukov and Parnachev, 1994). The magmatic rocks of the Byskarsk series are dated by the $^{40}Ar—^{39}Ar$ method as 392 Ma (Malkovets et al., 2003) and encompass flows of moderately alkaline basalts and basaltic trachyandesites, and in places dolerite sills. The proportion of sedimentary to magmatic rocks is 75:25%; up the section, the sedimentary proportion increases.

Having a similar structure, the Novosjelovsk area lies 30 km east of the Kopjevsk area (Fig. 4 and 5b). The sequence is over 800 m thick and largely consists of a series of flows of pyroxene and plagioclase porphyry basalts alternating with aphyric basalts and basaltic trachyandesites and scarce lenses of basalt tuff breccias and red siltstones.

3.2. Continuous volcanic association of Batenevsk area

The Batenevsk area separates two large depressions of the Minusinsk trough: Chebakov-Balakhtinsk and Syda-Erba (Figs. 4 and 6). Volcanics of the continuous association are present on the eastern
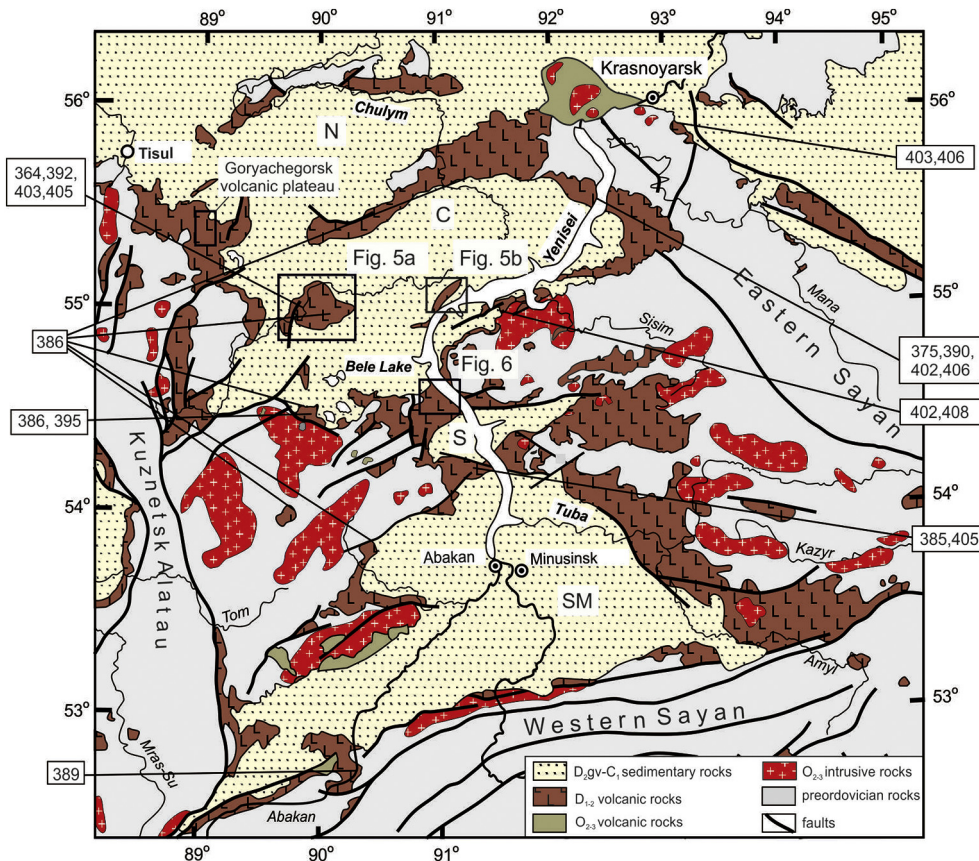

Fig. 4. Simplified geological scheme of the Early-Middle Paleozoic magmatic rock distribution in the Minusinsk trough (modified from Luchitsky, 1960) and location of Figs. 5a, b and 6. Depressions of the Minusinsk trough: SM = South-Minusinsk, S = Syda-Yerbinsk, C = Chebakov-Balakhtinsk, N = Nazarovsk. The numbers in rectangles indicate the age (Ma).
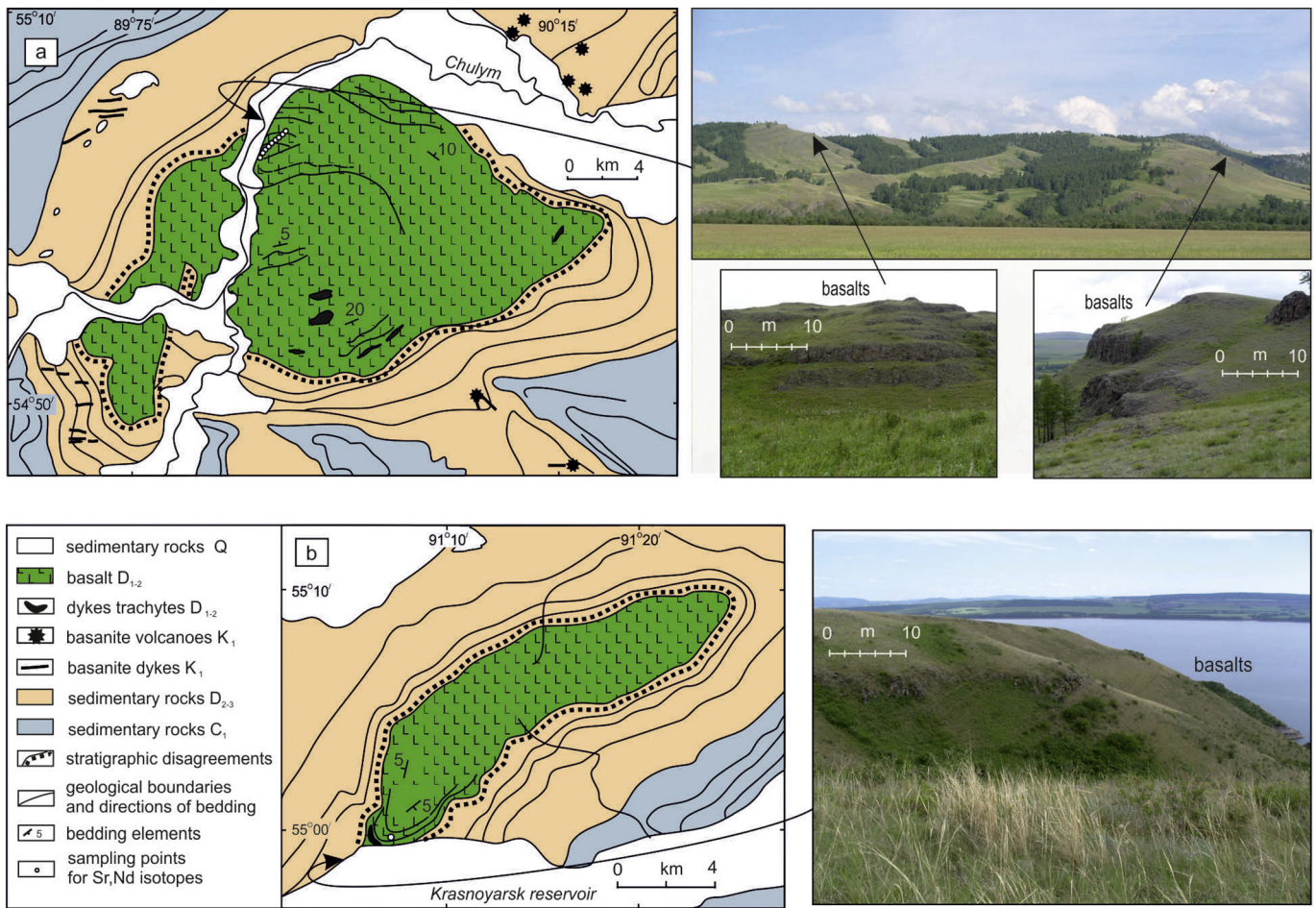
Fig. 5. Geological maps and representative photos of Devonian basalt flows in the Minusinsk trough: (a) Kopjevsk area; (b) Novosjelovsk area.

side with an area of over 600 km². The volcanic sequence of 700 m thickness overlies with angular unconformity the Cambrian-Ordovician basement. In turn sediments of the Zhivetian stage (Luchitsky, 1960) overlap the Batenevsk units. Schneider and Zubkus

(1962) referred to this volcanic sequence as the stratum type for the Early Devonian Byskarsk series of the Minusinsk depression.

The volcanic sequence consists of three rock series. Flows of aphyric, glassy and fine-grained basalts and basaltic trachyandesites comprise
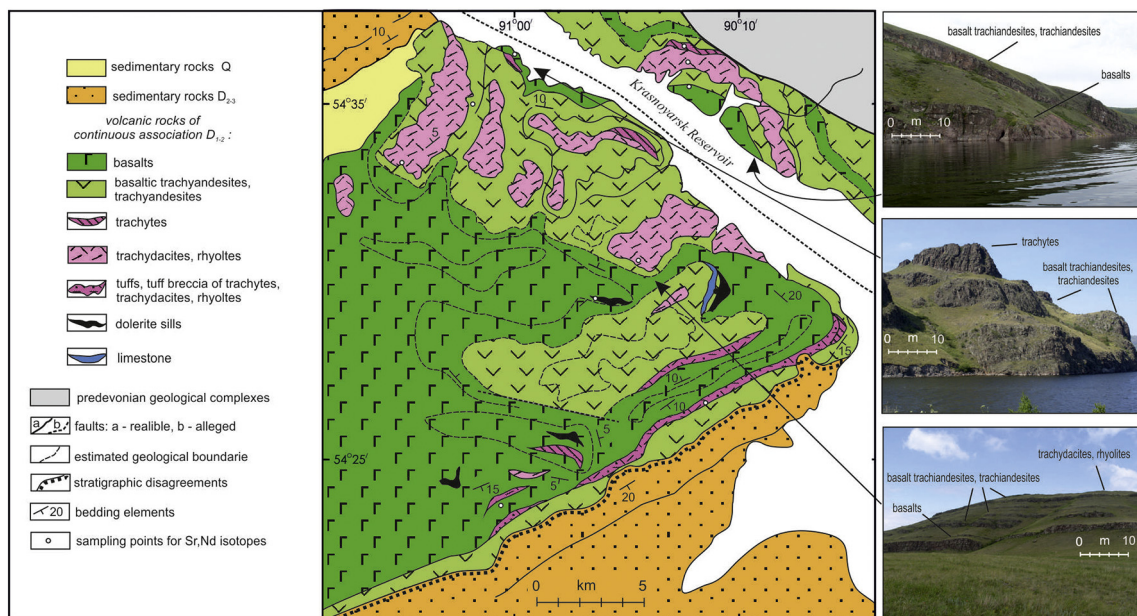
Fig. 6. Geological map and representative photos of Devonian rocks of the continuous association on the eastern side of the Batenevsk area in the Minusinsk trough.

Fig. 7. (a) Simplified structural-geological map of the Early Caledonian Lake Zone of northwestern Mongolia (modified from Vorontsov, 1993), illustrating the location of belts of grabens with the Devonian bimodal volcanic association and Khaldzan Buregte group of peralkaline massifs. Main grabens: SU = Shargatyn-Ula, BK = Bomiin-Khara, TK = Tsagan-Khairkhan, IG = Ichetuin-Gol, BE = Bayan-Erdenet. (b) Satellite spectrum-zonal photo of the Tsagan-Khairkhan graben and adjacent territory. (c) Geological map of t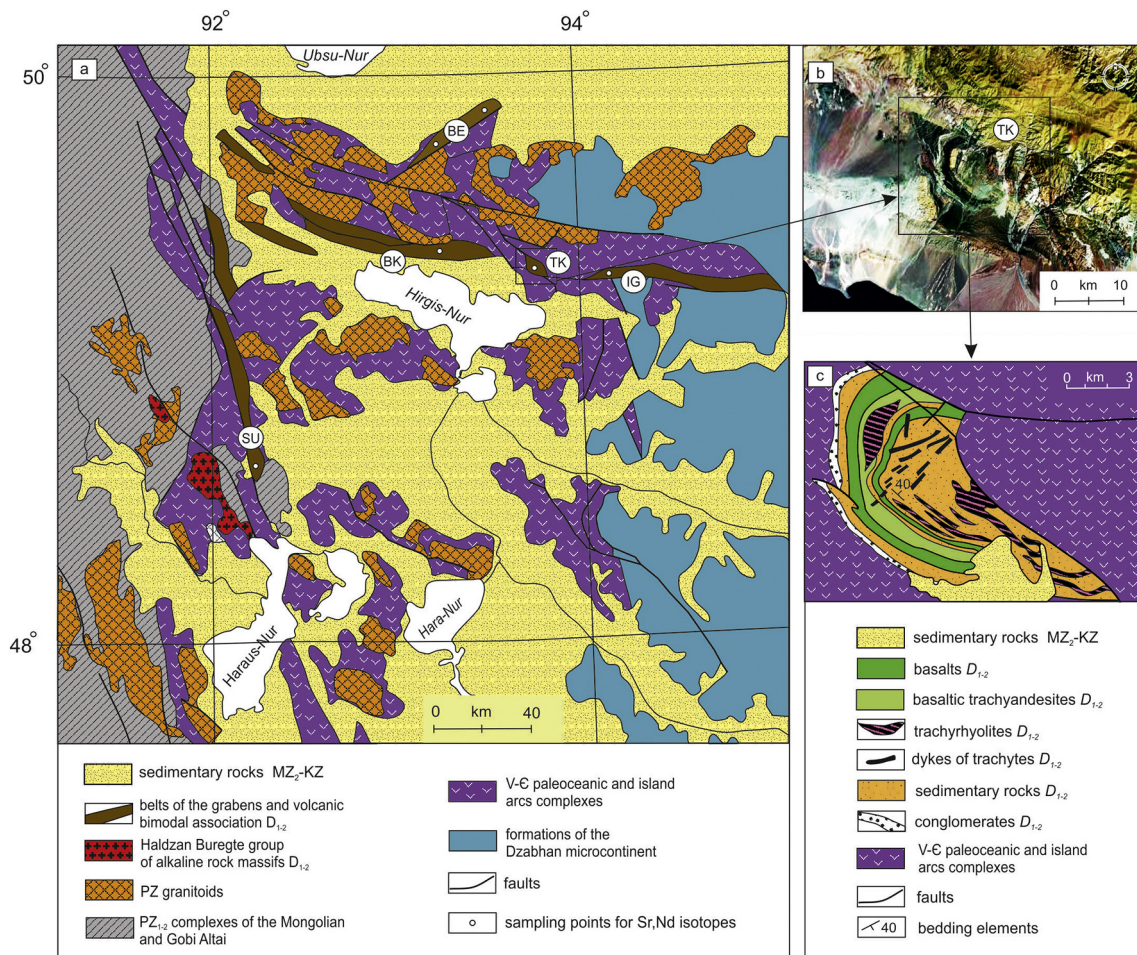he Tsagan-Khairkhan graben with terrigenous sediments and a bimodal volcanic association (reproduced from Yarmolyuk and Vorontsov, 1993).

the lower series. The lavas are interbedded with tuffs, tuff-breccias and tuff lavas, sandstones and siltstones which bear plant remains, conglomerates and rarely limestones. Some lava flows with thicknesses varying from 5 to 15 m resemble cuestas. The middle series of flows represent a greater range in composition: moderately alkaline basalts, trachyandesites, trachydacites and trachytes. This lava series also includes thin (from 0.5 to 2 m) interbeds and lenses of red sandstone, siltstone and limestone. The upper series of rock is outcroping in the center of the volcanic field and consists of flows and lenticular bodies of rhyolite and trachyte, in places separated by basalt flows.

In the Batenevsk area, the mafic rocks amount to 50% of the total volume, with trachyandesites at ~35%, trachytes and trachydacites at ~10%, and trachyrhyodacites and rhyolites at ~5%. $^{40}Ar—^{39}Ar$ dating of the Batenevsk volcanics gives an age range of 408–391 Ma (Vorontsov et al., 2015). Dolerite sills occur at different stratigraphic levels.

3.3. Alkaline volcanic association of Goryachegorsk plateau

The Goryachegorsk volcanic plateau sits at the junction of northeastern Kuznetsk Alatau with the western margin of the Minusinsk trough (Fig. 4). The plateau hosts Bazyrsk, Bereshsk and Ashpansk sequences (Markov, 1987; Uvarov and Uvarova, 2008) and discordantly overlies the Late Neo-Proterozoic – Early Paleozoic folded complexes. Alkaline volcanics compose part of the Bereshsk sequence, jointly with the

intrusions of differentiated alkaline gabbroids (Grinev, 1990; Vrublevsky et al., 2016).

The plateau includes a few distinct volcano-tectonic units. For instance, the Batanajul-Semjonovsk structure is a paleovolcano with external diameter about 40 km and cone-like outcrop about 2 km high. Moderately alkaline basalts and trachybasalts of the Bazyrsk sequence 1.0–1.5 km thick infill the paleo-volcano basement. The middle of the complicated Bereshsk sequence contains trachybasalts, basaltic trachyandesites, trachyandesites, trachytes and trachyrhyodacites, as well as alkaline rocks, e.g. nephelinite, tephrite, phonotephrite, tephriphonolite and phonolite. The outcrops produce a semi-ring like structure 24 km across; the thickness of volcanic rocks varies from 300 m t o 2.5 km. The elongate intrusive bodies of mafic foidolite and nepheline syenite pierce some volcanics of the Bereshsk sequence. The upper part of the Ashpansk sequence includes basalts, trachybasalts and trachytes with a minor amount of basanite. The composition of these rocks are similar to those of the Bazyrsk sequence. At the top, red terrigenous sediments of the Zhivetian stage occur.

3.4. Bimodal volcano-plutonic association of the Lake Zone grabens in northwestern Mongolia

In the Ichetuin-Gol (IG, Fig. 7a) and Bomiin-Khara (BK, Fig. 7a) areas of northwestern Mongolia sedimentary rocks are dominant, but igneous rocks are present at all stratigraphic level; cross-sections show flows of

Table 1
Major (wt%) and trace elements (ppm) in the rocks of the Devonian magmatic associations of ASRS.

Sample	Basalt association, Kopjevsk area						
	КОP1/1	KOP1/4	KOP1/5	KOP1/6	KOP1/8	KOP1/9	KOP1/10
SiO_2	47.58	48.25	47.84	46.93	47.47	46.35	49.50
TiO_2	1.05	1.27	1.51	1.77	1.09	1.38	1.24
Al_2O_3	15.79	16.07	16.37	16.95	16.54	16.17	17.62
Fe_2O_3t	10.07	9.98	11.09	11.25	9.30	10.04	9.37
MnO	0.16	0.20	0.18	0.41	0.24	0.12	0.17
MgO	9.26	6.46	6.62	5.79	7.09	7.19	5.20
CaO	9.63	8.39	8.41	8.19	9.83	8.95	8.91
Na_2O	3.49	3.95	4.33	3.51	2.96	3.42	3.73
K_2O	0.99	1.54	0.86	1.40	1.26	1.09	1.58
P_2O_5	0.38	0.54	0.62	0.75	0.48	0.48	0.52
LOI	1.73	3.57	2.36	3.21	3.54	4.96	2.15
Sum	100.29	100.40	100.37	100.34	100.27	100.33	100.28
$Na_2O + K_2O$	4.48	5.49	5.19	4.91	4.22	4.51	5.31
agp.c.							
Rb	18	25	5	13	12	7	14
Ba	483	685	1580	1452	4594	1793	3147
Sr	903	1079	1024	974	1139	866	1245
Zr	173	276	284	287	188	187	221
Nb	10.7	15.5	17.8	15.8	12.3	11.0	14.8
Hf	3.56	5.31	5.32	5.32	3.65	3.68	4.22
Ta	0.60	0.90	0.96	0.89	0.67	0.63	0.82
Y	24	29	30	32	22	24	25
Th	3.54	6.72	3.07	2.15	2.98	1.92	3.26
U	2.13	2.65	1.68	1.10	1.71	0.89	1.89
Pb	6.6	8.5	7.4	7.7	6.3	4.3	9.3
La	29	52	42	40	32	27	38
Ce	64	116	91	92	71	63	83
Pr	7.4	13.7	10.5	10.8	8.1	7.5	9.5
Nd	33	60	44	47	35	33	40
Sm	6.4	11.2	8.7	9.4	6.7	6.8	7.6
Eu	1.90	3.04	2.48	2.66	1.95	1.99	2.19
Gd	6.15	9.54	8.11	8.82	6.16	6.55	6.97
Tb	0.84	1.19	1.11	1.19	0.83	0.91	0.93
Dy	5.09	6.67	6.54	7.20	4.88	5.42	5.46
Ho	1.04	1.26	1.29	1.40	0.95	1.06	1.06
Er	3.16	3.70	3.66	3.95	2.68	3.06	3.02
Tm	0.42	0.48	0.51	0.56	0.38	0.42	0.42
Yb	2.72	3.15	3.34	3.69	2.57	2.73	2.73
Lu	0.42	0.48	0.52	0.55	0.39	0.41	0.43

Sample	Basalt association, Kopjevsk area			Continuous association, Batenevsk area			
	KOP1/11	KOP1/12	NVS1/5	BAT1/6	BAT4/11	BAT4/13	BAT1/28
SiO_2	47.50	51.55	51.21	48.67	53.30	49.51	47.84
TiO_2	1.18	1.58	1.55	1.27	1.42	1.44	1.17
Al_2O_3	18.15	17.29	17.47	16.35	17.26	19.41	17.36
Fe_2O_3t	10.13	11.56	8.44	11.34	8.32	9.57	10.86
MnO	0.15	0.13	0.42	0.15	0.16	0.18	0.13
MgO	6.17	2.80	3.69	3.66	3.01	3.45	5.45
CaO	8.22	5.65	4.80	9.92	7.46	6.74	9.16
Na_2O	3.42	4.52	6.04	3.41	3.56	3.75	3.44
K_2O	1.35	2.25	2.27	0.93	2.05	2.60	0.80
P_2O_5	0.44	0.73	0.84	0.27	0.66	0.43	0.33
LOI	3.23	2.03	3.21	3.99	2.74	2.86	3.52
Sum	100.14	100.33	100.21	100.11	100.16	100.21	100.32
$Na_2O + K_2O$	4.77	6.77	8.31	4.34	5.61	6.35	4.24
agp.c.							
Rb	13	21	25	12	51	70	8
Ba	1571	1858	1415	984	926	751	1994
Sr	1245	1057	1231	874	675	1128	878
Zr	137	291	382	118	259	153	137
Nb	8.2	20.6	26.1	6.3	15.4	9.4	6.2
Hf	2.84	5.69	6.96	2.90	6.25	3.99	2.97
Ta	0.45	1.22	1.47	0.51	0.87	0.56	0.41
Y	20	29	37	19	37	30	19
Th	2.14	4.91	5.65	2.00	9.44	4.58	3.79
U	1.20	1.64	2.71	0.88	2.98	1.60	1.43
Pb	7.7	10.7	7.3	5.3	12.4	8.8	6.3
La	27	46	55	16	52	36	30
Ce	60	100	121	36	114	78	62
Pr	7.2	11.6	13.7	4.8	13.3	9.6	7.5
Nd	32	49	58	23	55	41	34
Sm	6.0	9.0	10.7	5.0	10.4	8.1	7.0
Eu	1.85	2.42	3.00	1.54	2.90	2.57	1.73

Table 1 (*continued*)

Sample	Basalt association, Kopjevsk area			Continuous association, Batenevsk area			
	KOP1/11	KOP1/12	NVS1/5	BAT1/6	BAT4/11	BAT4/13	BAT1/28
Gd	5.69	8.26	10.01	4.92	9.71	7.81	6.56
Tb	0.75	1.10	1.36	0.70	1.52	1.25	0.80
Dy	4.47	6.48	8.06	4.35	7.54	6.01	4.93
Ho	0.86	1.29	1.57	0.88	1.51	1.18	0.93
Er	2.52	3.83	4.81	2.43	4.21	3.29	2.59
Tm	0.35	0.54	0.63	0.34	0.62	0.47	0.36
Yb	2.30	3.60	4.24	2.17	4.14	3.17	2.28
Lu	0.36	0.56	0.64	0.34	0.60	0.47	0.36

Sample	Continuous association, Batenevsk area						
	BAT3/13	BAT3/25	BAT3/5	BAT3/23	BAT4/3	BAT4/4	BAT4/14
SiO_2	51.49	47.72	49.86	48.66	50.24	50.99	52.34
TiO_2	1.50	1.14	2.15	1.56	1.92	1.84	1.73
Al_2O_3	16.41	18.78	15.57	17.45	15.34	15.92	15.64
Fe_2O_3t	10.44	10.09	11.83	11.63	11.47	11.42	10.93
MnO	0.15	0.16	0.21	0.19	0.18	0.19	0.25
MgO	3.87	4.94	4.09	4.59	3.49	2.84	3.27
CaO	7.39	10.75	6.61	9.31	9.40	7.21	5.29
Na_2O	3.81	3.31	5.25	3.41	3.36	3.75	3.38
K_2O	2.47	0.92	1.76	1.01	0.88	2.11	3.51
P_2O_5	0.48	0.26	0.93	0.45	0.60	1.17	0.86
LOI	2.06	2.06	1.90	1.90	3.28	2.53	2.71
Sum	100.33	100.28	100.35	100.32	100.33	100.20	100.19
$Na_2O + K_2O$	6.28	4.23	7.01	4.42	4.24	5.86	6.89
agp.c.							
Rb	54	17	35	17	14	52	71
Ba	955	316	748	380	457	699	1229
Sr	961	814	828	727	627	954	911
Zr	228	97	191	145	145	170	274
Nb	14.9	7.0	14.0	7.3	7.9	9.7	15.4
Hf	5.49	2.59	4.66	3.60	3.72	4.36	6.78
Ta	0.85	0.42	0.78	0.36	0.45	0.56	0.91
Y	33	21	43	32	33	41	50
Th	3.99	1.89	3.94	2.22	3.16	4.84	7.34
U	1.63	0.87	1.73	0.84	1.02	1.75	2.53
Pb	9.2	4.2	7.7	4.8	6.3	8.5	9.9
La	32	18	43	26	27	40	55
Ce	73	41	100	63	66	95	124
Pr	8.9	5.3	12.6	7.9	8.7	12.1	15.0
Nd	37	23	55	34	38	55	66
Sm	7.7	4.8	10.8	7.1	8.0	11.2	12.8
Eu	2.01	1.59	3.35	2.19	2.52	3.48	3.72
Gd	7.38	4.82	10.78	7.05	7.86	10.98	12.87
Tb	1.10	0.79	1.67	1.13	1.25	1.67	1.99
Dy	6.30	4.29	8.56	6.20	6.72	8.84	9.88
Ho	1.31	0.88	1.71	1.26	1.33	1.71	1.99
Er	3.57	2.43	4.69	3.58	3.60	4.65	5.52
Tm	0.52	0.36	0.67	0.52	0.51	0.67	0.81
Yb	3.37	2.42	4.42	3.46	3.41	4.33	5.45
Lu	0.52	0.36	0.63	0.50	0.47	0.62	0.78

Sample	Continuous association, Batenevsk area						
	BSK1/11	BAT1/8	BAT5/9	BSK1/6	BAT1/25	BAT3/24	BAT3/26
SiO_2	49.60	64.59	57.61	57.50	64.51	72.38	71.54
TiO_2	2.10	0.58	1.30	1.29	0.94	0.43	0.57
Al_2O_3	14.85	14.56	15.86	16.21	15.73	13.93	14.09
Fe_2O_3t	12.89	5.78	7.70	7.52	5.61	2.36	2.66
MnO	0.24	0.11	0.22	0.21	0.14	0.02	0.03
MgO	4.47	0.43	2.06	2.16	0.57	0.26	0.44
CaO	5.73	1.10	4.22	3.70	1.13	1.15	1.41
Na_2O	5.63	4.96	4.70	5.25	6.35	4.70	5.35
K_2O	1.12	3.73	2.95	2.50	3.04	4.09	3.06
P_2O_5	0.92	0.11	0.49	0.59	0.21	0.05	0.11
LOI	2.46	3.88	2.79	3.06	1.78	0.48	0.70
Sum	100.29	100.07	100.10	100.17	100.17	100.06	100.14
$Na_2O + K_2O$	6.75	8.69	7.65	7.75	9.39	8.79	8.41
agp.c.		0.79			0.76	0.85	0.77
Rb	15	83	73	61	57	91	65
Ba	751	2025	884	619	837	1014	874
Sr	1338	534	663	460	341	225	320
Zr	123	638	363	198	392	398	276
Nb	6.1	34.5	22.2	12.1	21.6	21.6	19.3

Table 1 (*continued*)

Sample	Continuous association, Batenevsk area						
	BSK1/11	BAT1/8	BAT5/9	BSK1/6	BAT1/25	BAT3/24	BAT3/26
Hf	3.33	13.70	8.76	5.21	9.39	9.68	7.85
Ta	0.36	2.57	1.37	0.87	1.27	1.38	1.54
Y	38	56	45	34	47	46	30
Th	2.52	14.48	8.93	7.19	9.80	14.34	11.18
U	0.82	3.71	3.94	2.73	2.75	3.86	4.79
Pb	6.2	12.6	16.1	6.1	14.1	10.5	5.8
La	33	66	57	36	55	38	30
Ce	79	148	117	86	120	88	76
Pr	10.8	17.3	14.3	10.8	15.5	10.8	9.4
Nd	51	69	58	46	60	43	39
Sm	10.9	13.1	10.3	9.3	11.8	9.1	7.7
Eu	3.78	2.69	2.34	2.77	3.16	1.99	1.89
Gd	10.90	11.78	8.47	8.98	10.93	9.24	7.90
Tb	1.61	1.80	1.24	1.39	1.77	1.51	1.05
Dy	7.97	11.54	9.27	7.00	9.65	8.72	6.15
Ho	1.50	2.40	1.86	1.32	2.10	1.80	1.18
Er	4.09	7.25	5.48	3.75	5.51	5.32	3.33
Tm	0.57	1.09	0.81	0.56	0.87	0.84	0.49
Yb	3.73	7.34	5.27	3.74	5.55	5.68	3.28
Lu	0.52	1.20	0.80	0.55	0.92	0.86	0.51

Sample	Continuous association, Batenevsk area						
	BAT 4/2	BAT5/1	BAT1/3	BAT1/18	BAT1/32	BAT3/9	BAT4/5
SiO_2	68.52	60.21	60.08	67.20	69.65	54.57	69.39
TiO_2	0.41	1.32	1.29	0.63	0.57	1.19	0.50
Al_2O_3	15.22	15.27	14.42	14.31	14.44	17.81	14.67
Fe_2O_3t	3.09	7.25	6.18	3.91	3.82	8.97	3.68
MnO	0.17	0.15	0.13	0.09	0.13	0.14	0.06
MgO	0.50	1.83	1.32	0.41	0.23	2.28	0.31
CaO	1.53	3.09	2.91	0.64	0.68	6.59	1.16
Na_2O	5.06	4.40	4.51	5.18	5.05	4.21	5.65
K_2O	4.05	3.53	3.21	4.87	4.80	2.05	3.80
P_2O_5	0.08	0.54	0.44	0.11	0.11	0.41	0.07
LOI	1.32	2.20	5.63	2.54	0.60	1.77	0.68
Sum	100.20	100.00	100.30	100.16	100.21	100.28	100.12
$Na_2O + K_2O$	9.11	7.93	7.72	10.05	9.85	6.26	9.45
agp.c.	0.80			0.95	0.93		0.84
Rb	89	100	102	73	98	39	92
Ba	1478	844	657	2036	521	1369	575
Sr	375	646	579	216	178	873	282
Zr	353	376	330	446	480	162	486
Nb	20.5	21.0	20.3	22.6	24.2	9.1	27.8
Hf	9.50	9.52	8.17	10.00	11.35	4.42	13.30
Ta	1.38	1.41	1.31	1.79	1.54	0.61	1.89
Y	44	45	43	44	55	32	61
Th	10.12	13.82	10.78	11.21	13.49	5.32	13.95
U	2.78	5.46	3.16	3.44	3.48	2.05	3.94
Pb	9.8	15.8	13.6	27.0	19.1	9.7	16.8
La	53	56	52	53	69	33	48
Ce	114	123	116	106	146	74	99
Pr	13.4	15.2	14.0	13.5	18.6	9.3	11.3
Nd	54	60	58	57	69	39	46
Sm	9.6	11.6	11.2	11.9	12.7	7.9	8.9
Eu	2.30	2.45	2.55	2.77	2.31	2.59	1.81
Gd	9.74	9.81	10.25	10.51	11.35	7.62	9.77
Tb	1.38	1.62	1.46	1.61	1.91	1.18	1.58
Dy	8.21	9.59	8.26	9.87	10.92	6.24	10.30
Ho	1.62	1.88	1.63	2.02	2.45	1.26	2.28
Er	4.94	5.29	4.47	5.90	6.43	3.52	7.08
Tm	0.74	0.78	0.64	0.88	1.05	0.52	1.04
Yb	5.04	4.96	3.99	5.89	6.81	3.42	7.20
Lu	0.80	0.78	0.62	0.92	1.13	0.50	1.14

Sample	Continuous association, Batenevsk area				Alkaline association, Goryachegorsk plateau		
	BAT4/10	BAT5/8	BAT1/12	BSK1/5	BRS1/3	BRS2/6	URP1/6
SiO_2	54.95	62.60	74.07	76.63	58.25	45.09	48.03
TiO_2	1.40	0.83	0.31	0.21	0.38	0.49	0.37
Al_2O_3	16.90	16.39	11.23	11.59	18.65	22.79	23.05
Fe_2O_3t	8.52	5.13	2.78	2.15	4.94	8.52	6.27
MnO	0.14	0.12	0.03	0.03	0.15	0.20	0.15
MgO	2.46	1.75	0.29	0.29	0.81	1.20	0.67
CaO	7.08	3.07	0.53	1.00	1.79	5.14	6.67
Na_2O	3.60	4.37	4.69	3.75	6.43	8.11	7.08

Table 1 (*continued*)

Sample	Continuous association, Batenevsk area				Alkaline association, Goryachegorsk plateau		
	BAT4/10	BAT5/8	BAT1/12	BSK1/5	BRS1/3	BRS2/6	URP1/6
K_2O	2.23	3.26	2.34	3.28	5.41	1.96	3.36
P_2O_5	0.65	0.28	0.10	0.07	0.09	0.25	0.22
LOI	2.00	2.05	3.55	0.91	3.08	6.29	4.05
Sum	100.12	100.04	100.06	100.09	100.11	100.52	100.48
$Na_2O + K_2O$	5.83	7.63	7.03	7.03	11.84	10.07	10.44
agp.c.			0.80	0.82			
Rb	63	104	38	58	147	25	69
Ba	646	820	1479	1232	316	2530	1246
Sr	672	763	229	149	299	2744	5185
Zr	263	269	179	161	656	315	227
Nb	14.8	16.1	9.8	12.6	70.8	43.0	36.9
Hf	6.29	6.33	4.27	4.23	13.30	3.47	2.36
Ta	0.89	1.19	1.32	1.15	3.67	2.43	1.73
Y	39	29	12	10	44	32	24
Th	9.84	12.78	12.22	9.59	26.97	6.60	11.06
U	3.09	3.53	5.19	2.56	10.37	6.24	3.55
Pb	11.3	18.0	13.8	5.3	36.0	12.5	17.9
La	53	44	26	12	75	48	40
Ce	117	91	51	25	126	96	70
Pr	13.6	10.8	5.3	3.2	13.2	10.0	6.6
Nd	56	41	20	12	43	38	22
Sm	10.7	7.4	3.4	2.2	6.7	6.5	3.7
Eu	2.84	1.66	0.74	0.49	0.77	2.12	1.53
Gd	10.15	6.20	2.75	2.03	5.85	6.23	4.85
Tb	1.58	0.84	0.40	0.35	0.95	0.92	0.53
Dy	7.85	6.21	2.53	1.93	6.14	6.00	3.66
Ho	1.56	1.17	0.50	0.43	1.62	1.31	0.76
Er	4.25	3.42	1.44	0.79	4.89	4.39	2.46
Tm	0.63	0.48	0.22	0.19	0.87	0.62	0.37
Yb	4.18	3.12	1.50	1.34	5.42	4.30	2.56
Lu	0.61	0.47	0.25	0.23	0.81	0.63	0.38

Sample	Alkaline association, Goryachegorsk plateau						Bimodal association, Mongolia
	URP2/5	URP2/6	URP2/8	URP2/9	URP2/10	URP2/47	KNK2/9
SiO_2	53.93	52.51	46.04	50.02	49.31	62.44	49.47
TiO_2	0.75	0.91	1.91	1.47	1.46	0.55	2.17
Al_2O_3	20.89	20.80	17.16	17.73	18.06	15.81	17.66
Fe_2O_3t	7.59	9.21	13.94	11.68	12.56	7.34	8.92
MnO	0.16	0.22	0.27	0.21	0.25	0.13	0.08
MgO	1.56	1.27	2.43	1.55	1.58	0.28	3.60
CaO	4.22	4.74	6.55	5.08	5.06	0.96	3.60
Na_2O	6.76	6.43	6.69	7.26	7.65	6.44	4.76
K_2O	3.18	2.26	2.22	1.97	2.59	4.87	3.36
P_2O_5	0.34	0.60	1.33	0.75	0.90	0.07	0.90
LOI	1.08	0.96	0.98	2.15	0.47	0.90	4.63
Sum	100.61	100.09	99.68	100.07	100.06	99.87	99.65
$Na_2O + K_2O$	9.93	8.69	8.91	9.22	10.24	11.31	8.12
agp.c.							
Rb	63	41	38	26	44	131	49
Ba	790	818	778	850	750	179	924
Sr	612	749	804	616	545	46	638
Zr	504	554	463	622	538	955	267
Nb	39.4	41.5	30.1	38.9	34.8	49.7	46.5
Hf	8.96	9.46	7.77	10.20	9.02	20.82	5.06
Ta	2.57	2.47	1.84	2.42	2.23	3.07	2.81
Y	35	49	57	53	64	93	22
Th	9.52	8.77	6.34	9.08	7.56	15.32	3.02
U	29.42	5.40	5.70	7.57	6.34	9.15	1.61
Pb	50.7	23.3	11.4	8.8	7.0	33.5	47.3
La	42	50	52	52	56	76	40
Ce	84	108	119	112	126	157	84
Pr	9.5	12.8	15.0	13.5	15.3	18.9	10.4
Nd	35	48	61	53	62	74	43
Sm	6.5	9.8	12.2	10.7	12.8	16.1	8.6
Eu	2.10	2.89	3.68	2.97	3.61	2.09	3.13
Gd	6.37	8.98	11.61	10.46	12.29	15.67	8.13
Tb	1.15	1.58	1.95	1.75	2.10	2.78	1.22
Dy	7.01	9.75	11.37	10.53	12.51	18.05	5.37
Ho	1.57	2.06	2.34	2.28	2.58	3.80	0.94
Er	5.04	6.41	6.87	7.04	7.94	12.34	2.66
Tm	0.79	0.99	1.03	1.05	1.17	1.86	0.32
Yb	5.42	6.65	6.60	7.25	7.80	12.59	1.94
Lu	0.79	1.04	0.96	1.11	1.17	1.98	0.27

Sample	Bimodal association, Mongolia							
	KNK 1/2	KNK 5/30	KNK 10/3	KNK 11/2	KBU 3/12	BMH 05/31	BMH 05/32	BMH 05/32a
SiO_2	45.61	47.11	43.91	47.21	49.46	69.80	70.19	67.53
TiO_2	2.50	3.59	4.05	2.64	2.59	0.23	0.24	0.34
Al_2O_3	16.92	15.33	15.80	17.15	17.14	12.47	12.27	13.86
Fe_2O_3t	11.95	12.01	13.60	11.81	9.68	5.24	5.17	5.39
MnO	0.16	0.20	0.24	0.17	0.30	0.10	0.10	0.13
MgO	5.36	4.57	4.91	3.37	3.99	0.12	0.07	0.19
CaO	8.57	5.79	8.82	7.70	6.49	0.40	0.32	0.64
Na_2O	2.83	3.78	3.42	3.78	4.42	6.77	6.16	6.46
K_2O	1.16	1.61	0.85	2.00	1.44	4.17	4.08	4.64
P_2O_5	0.43	0.72	0.74	0.75	0.79	0.02	0.02	0.04
LOI	3.06	3.82	2.15	2.06	2.62	0.59	0.52	0.59
Sum	99.13	99.99	99.58	99.51	99.68	99.31	98.62	99.22
$Na_2O + K_2O$	3.99	5.39	4.27	5.78	5.86	10.94	10.24	11.10
agp.c.						1.25	1.19	1.13
Rb	11	19	11	28	25	159	152	131
Ba	238	394	290	709	539	22	27	16
Sr	659	537	784	840	785	10	8	9
Zr	210	290	225	246	398	1610	1810	1550
Nb	23.6	35.2	32.7	52.3	52.0	198.0	244.0	213.0
Hf	4.28	5.55	4.63	5.16	7.53	41.10	45.20	39.70
Ta	1.74	2.23	2.22	2.97	3.44	16.90	19.70	16.70
Y	21	31	26	29	32	117	147	127
Th	1.77	2.50	1.95	3.87	4.86	27.20	33.60	28.90
U	0.54	0.76	0.64	1.11	1.41	7.99	9.02	7.22
Pb	3.9	6.2	3.6	7.5	7.8	23.0	35.1	28.2
La	22	34	30	43	46	143	186	158
Ce	46	75	65	84	94	284	372	312
Pr	6.1	9.7	8.4	10.2	11.6	33.6	41.7	36.9
Nd	26	42	35	42	46	121	155	135
Sm	5.7	9.2	7.7	8.6	9.1	25.0	32.7	28.5
Eu	2.04	2.94	2.73	2.92	3.30	0.69	0.85	0.87
Gd	6.04	8.89	8.01	8.50	10.08	22.90	29.10	25.70
Tb	0.93	1.40	1.24	1.33	1.57	3.52	4.54	4.09
Dy	4.59	6.57	5.93	6.25	7.02	21.80	27.30	25.30
Ho	0.84	1.22	1.08	1.16	1.35	4.14	5.36	4.79
Er	2.34	3.46	2.96	3.32	4.03	12.60	16.90	13.70
Tm	0.29	0.43	0.36	0.41	0.51	1.88	2.54	2.13
Yb	1.86	2.74	2.22	2.60	3.39	13.20	16.20	13.30
Lu	0.26	0.38	0.30	0.36	0.49	1.74	2.20	1.77

Note: (1) Fe_2O_3t represents total iron; (2) agp.c. = agpaitic coefficient (molecular ratio of $(Na_2O + K_2O)/Al_2O_3$) from Le Maitre et al. (1997).

aphyric olivine basalts, trachyrhyolites, pantellerites, and also sills, dykes and stocks of teshenites and alkaline micro granites. A thick (about 50 m) sill of fine-grained alkaline nepheline syenite (mariupolite) is present in the middle of the Bomiin-Khara cross-section. The Tsagan-Khairkhan volcanic field (TK, Fig. 7a,b,c) contains rocks of the bimodal association, which combines trachybasalts of the lower section and trachytes, alkaline trachydacites and pantellerites in its upper part. The Bayan-Erdenet area (BE, Fig. 7a) hosts only basalts, in which aphyric fine-grained varieties prevail over porphyritic ones. In Shargatyn-Ula (SU, Fig. 7a) contains volcanics which consist of alternating units of a bimodal trachybasalt-pantellerite association. Infrequent sills of trachydolerite occupy the lower parts of the section.

The Khaldzan Buregte group of massifs (Fig. 7a) consists of moderately alkaline dolerite, alkaline basite, syenite, nordmarkite, peralkaline granite, pantellerite, ekerite and rare-metal peralkaline granite.

4. Analytical methods

4.1. Whole-rock compositions

Major and rare elements were analyzed at the Center for Collective Use (CCU) "Isotope-Geochemical Research", Institute of Geochemistry, Siberian Branch of the Russian Academy of Sciences, Irkutsk. Major elements were analyzed by XRF with a CPM-25 multichannel spectrometer, as described by Afonin et al. (1984). Measurements of rare elements were performed by the ICP-MS method on a ELEMENT-2

Finnigan MAT high-resolution mass spectrometer. To address possible matrix effects and to consider instability in the spectra (XRF) the analysts used the internal standard Rh. To calibrate the calculations of elemental contents in ICPMS measurements, multi-element certified solutions CLMS-1, −2, −4, SPEX (the USA) were applied. Rock samples of mafic and intermediate composition were prepared by open acid decomposition, and samples of felsic volcanics were prepared by fusion with Li-metaborate.

4.2. Isotopes

The samples were chemically prepared for isotope analyses in clean rooms at the CCU "Isotope-Geochemical Research", Institute of Geochemistry, Siberian Branch of the Russian Academy of Sciences, Irkutsk. Pure fractions of Sr were recovered from geological samples by the 2-stage scheme with ion-exchangeable resins BioRad AG 50 W*8, 200–400 mesh and BioRad AG 50*12, 200–400 mesh. To determine the isotope composition of strontium and Rb/Sr concentrations the analysts applied the method of isotope dilution and mixed tracer $^{85}Rb + ^{84}Sr$.

Pure Nd fractions were recovered with ion-exchangeable resins BioRad AG-50Wx12 200–400 mesh to get the sum of rare earths, and LN-Eicrome to obtain pure Nd and Sm fractions. To determine the isotope composition of neodymium and Nd/Sm concentrations the analysts applied the method of isotope dilution and mixed tracer $^{149}Sm + ^{150}Nd$.

The isotopic composition of Sr and Nd were measured in the static mode by the Finnigan 7-collector mass spectrometer MAT-262 in the
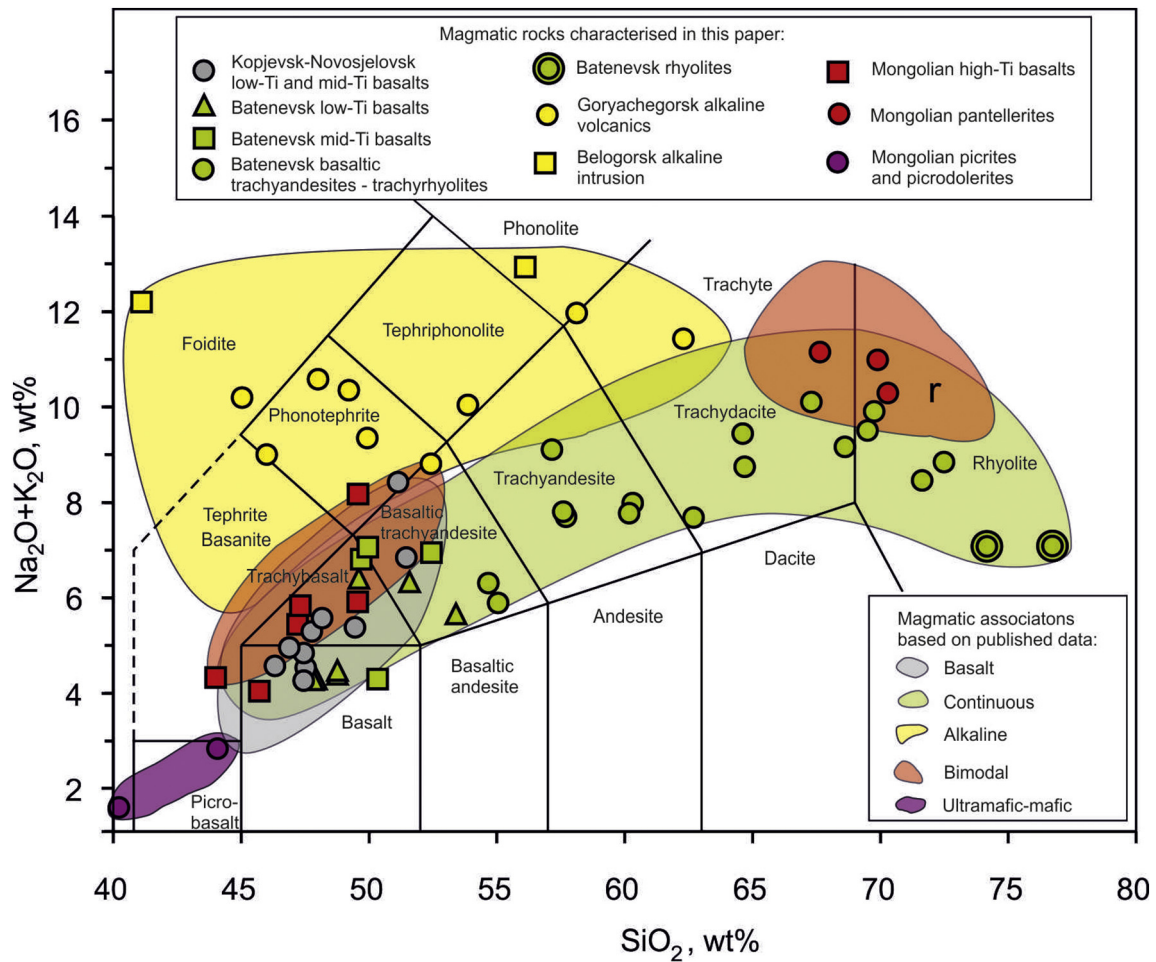
Fig. 8. Total alkalis vs. silica (TAS) diagram (Le Bas et al., 1986) showing the heterogeneous composition of Devonian magmatic rocks and associations of the Altai-Sayan Rift System. Magmatic associations: basaltic (reproduced from Zubkov et al. (1986), Lavrenchuk et al. (2004), Fedoseev (2008), Vorontsov et al. (2011)); continuous (reproduced from Babin et al. (2004), Vorontsov et al. (2015, 2018), Krupchatnikov et al. (2018)); alkaline (reproduced from Yashina (1982), Markov (1987), Grinev (2007), Uvarov and Uvarova (2008, 2009), Vrublevsky et al. (2016)); bimodal (reproduced from Yarmolyuk and Kovalenko (1991), Yarmolyuk and Vorontsov (1993), Vorontsov (1993), Kovalenko et al. (1989, 2004a, 2004b), Kruk et al. (2008)); ultramafic-mafic (reproduced from Izokh et al. (2011)).

CCU for "Geodynamics and Geochronology" at the Institute of the Earth's Crust, Siberian Branch of the Russian Academy of Sciences, Irkutsk. For measuring the isotopic Sr composition, the single-band configuration of the ion source was employed. The sample, weighing 50 ng, was placed on the Ta or Re cathode, on which the Ta pentoxide-based activator was preliminarily deposited. The ion current [88]Sr was usually equal to $2-3 * 10 (-11)$ A. The measured isotope ratios were normalized by the value of $^{88}Sr/^{86}Sr = 8.37521$. The presence of Rb interference in ^{87}Sr was corrected with $^{87}Rb/^{85}Rb = 0.386$. The accuracy of measured isotopic composition was estimated with measurements on standard samples NBS-987 and BCR-2 (the USA), with the amounts of $^{87}Sr/^{86}Sr = 0.710254 \pm 7$ ($2\sigma, n = 45$) and $^{87}Sr/^{86}Sr = 0.705011 \pm 14$ ($2\sigma, n = 7$), respectively. The Nd isotope composition was measured from the 2-band ion source based on Re cathodes. The amount of the applied sample averaged 100–200 ng. The ion current of ^{146}Nd was usually equal to $0.5-1.0 * 10 (-11)$ A. The presence of Sm interference in the Nd spectrum was controlled by the ratio $^{147}Sm/^{144}Nd$, lower 0.00005. The presence of ^{144}Sm in ^{144}Nd was corrected with respect to $^{144}Sm/^{147}Sm = 0.20504$. The measured $^{143}Nd/^{144}Nd$ isotopic ratios were normalized to the ratio $^{146}Nd/^{144}Nd = 0.7219$. The accuracy of the isotopic data were estimated from the results of measuring standard samples BCR-2 and JNdi-1 (the USA), which have values of $^{143}Nd/^{144}Nd = 0.512629 \pm 8$ ($2\sigma, n = 18$) and $^{143}Nd/^{144}Nd = 0.512107 \pm 4$ ($2\sigma, n = 35$), respectively. The

values of εNd and εSr were calculated relative to the model chondrite reservoir CHUR with the parameters $^{143}Nd/^{144}Nd = 0.512638$; $^{147}Sm/^{144}Nd = 0.1967$; $^{87}Rb/^{86}Sr = 0.7045$; $^{87}Sr/^{86}Sr = 0.0816$ (Faure, 1986).

5. Results

Fifty-eight volcanic rock samples were analyzed for major and trace element abundances; the results are listed in Table 1. These include basalt - 10, continuous sequence- 30, alkaline - 9, and bimodal - 9. These data were augmented by literature data for intrusive rocks of the bimodal (Kovalenko et al., 2004b), alkaline (Vrublevsky et al., 2016) and ultramafic-mafic associations (Izokh et al., 2011). Fig. 8 provides the TAS classification (Total Alkalis vs. Silica).

5.1. TAS classification and petrography

5.1.1. Basalt association

The basalt association of the Kopjevsk and Novosjelovsk areas predominantly contains basalts, trachybasalts and basaltic trachyandesites. They typically contain Na$_2$O + K$_2$O ~ 4.2–6.8 wt% with SiO$_2$ ~ 46.4–51.6- wt%. In places, there are intermediate basaltic trachyandesite-phonotephrites with Na$_2$O + K$_2$O = 8.3 wt%, and SiO$_2$ = 51.2 wt%. All the basalts are split into two groups by TiO$_2$ content: low-Ti
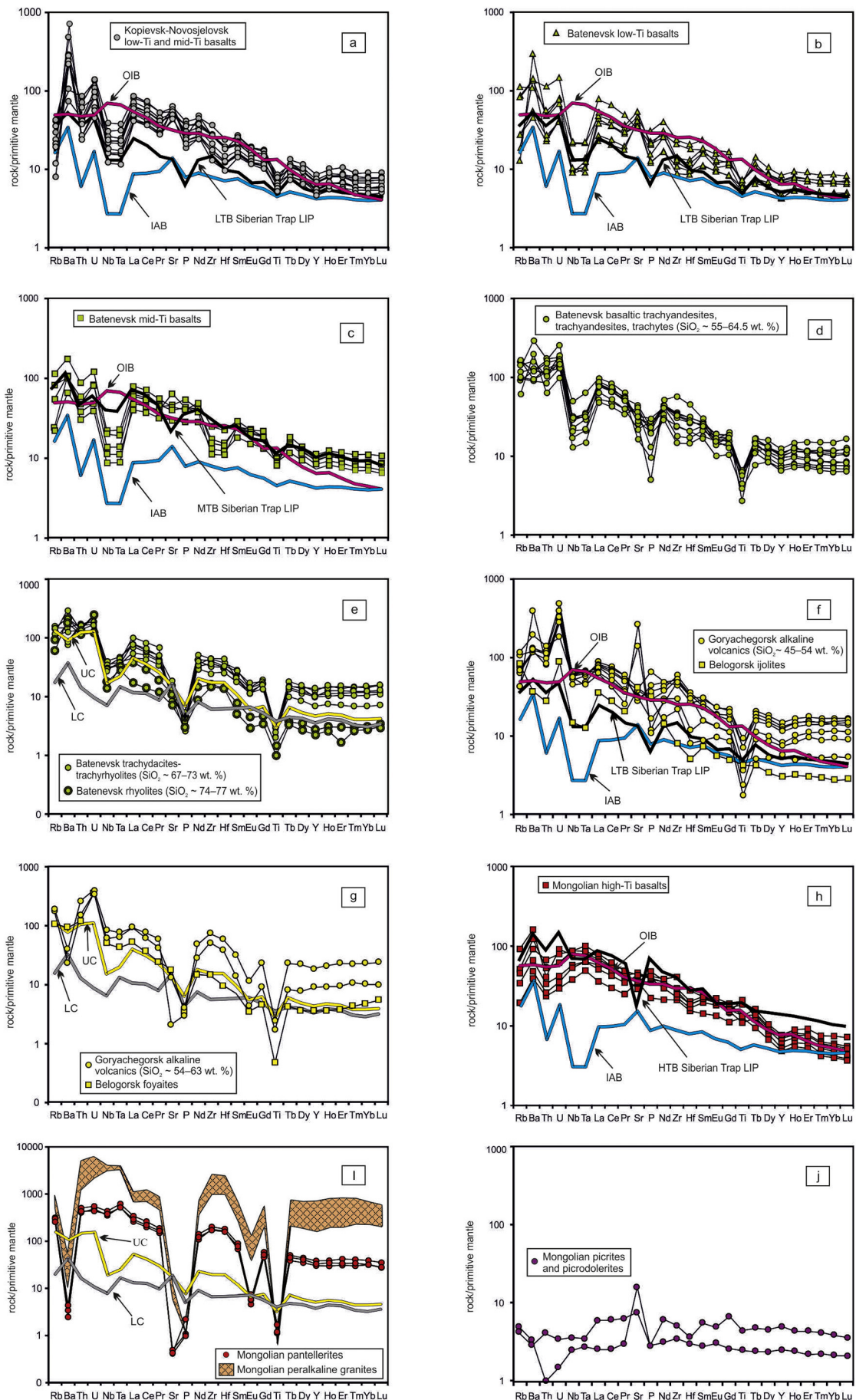
Table 2
Rb-Sr isotope composition for representative rocks of the ASRS Devonian magmatic associations.

Sample	Association type	Rock type	$^{87}Rb/^{86}Sr$	$^{87}Sr/^{86}Sr$	Err (2σ)	$\varepsilon_{Sr}(0)$	$\varepsilon_{Sr}(395)$
KOP 1/1	Basalt	Low-ti basalt	0.057616	0.704969	14	6.7	8.6
KOP 1/4	Basalt	Low-ti basalt	0.066969	0.705080	16	8.2	9.4
KOP 1/5	Basalt	Low-ti basalt	0.014113	0.704509	9	0.1	5.5
KOP 1/6	Basalt	Mid-ti basalt	0.038578	0.704619	10	1.7	5.1
KOP 1/8	Basalt	Low-ti basalt	0.030452	0.704942	11	6.3	10.4
KOP 1/9	Basalt	Low-ti basalt	0.023363	0.704742	10	3.4	8.1
KOP 1/10	Basalt	Low-ti basalt	0.032502	0.704708	15	3.0	6.9
KOP 1/11	Basalt	Low-ti basalt	0.030181	0.704659	20	2.3	6.4
KOP 1/12	Basalt	Mid-ti basalt	0.057425	0.705062	15	8.0	9.9
NVS 1/5	Basalt	Low-ti basalt	0.058700	0.705255	11	10.7	12.6
BAT 1/6	Continuous	Low-ti basalt	0.038301	0.704752	15	3.6	7.0
BAT 4/11	Continuous	Low-ti basalt	0.219970	0.705772	13	18.1	7.0
BAT 4/13	Continuous	Low-ti basalt	0.178877	0.705607	15	15.7	8.0
BAT 3/5	Continuous	Mid-ti basalt	0.120621	0.705120	16	8.8	5.7
BAT 3/23	Continuous	Mid-ti basalt	0.068942	0.704850	15	5.0	6.0
BAT 1/8	Continuous	Trachyte	0.449255	0.707350	13	40.5	11.1
BAT 4/2	Continuous	Trachydacites	0.685985	0.708440	12	55.9	7.7
BAT 5/1	Continuous	Trachyandesite	0.447429	0.707200	12	38.3	9.1
BAT 1/12	Continuous	Rhyolite	0.479628	0.707910	12	48.4	16.6
BSK 1/5	Continuous	Rhyolite	1.125118	0.711820	11	103.9	20.6
KHK 2/9	Bimodal	High-Ti basalt	0.221989	0.705373	16	12.4	1.2
KHK 1/2	Bimodal	High-Ti basalt	0.048246	0.703355	18	−16.3	−13.6
KHK 5/30	Bimodal	High-Ti basalt	0.102267	0.704067	10	−6.1	−7.8
KHK 10/3	Bimodal	High-Ti basalt	0.040185	0.703555	20	−13.4	−10.1
KHK 11/2	Bimodal	High-Ti basalt	0.096346	0.704000	13	−7.1	−8.3
KBU 3/12	Bimodal	High-Ti basalt	0.092787	0.704478	22	−0.3	−1.2

Table 3
Sm–Nd isotope composition for representative rocks of the ASRS Devonian magmatic associations.

Sample	Association type	Rock type	$^{147}Sm/^{144}Nd$	$^{143}Nd/^{144}Nd$	Err (2σ)	$\varepsilon_{Nd}(0)$	$\varepsilon_{Nd}(395)$
KOP 1/1	Basalt	Low-Ti basalt	0.116734	0.512672	11	0.7	4.7
KOP 1/4	Basalt	Low-Ti basalt	0.112356	0.512739	7	2.0	6.2
KOP 1/5	Basalt	Low-Ti basalt	0.119014	0.512651	10	0.3	4.2
KOP 1/6	Basalt	Mid-Ti basalt	0.120382	0.512712	7	1.4	5.3
KOP 1/8	Basalt	Low-Ti basalt	0.115223	0.512672	4	0.7	4.8
KOP 1/9	Basalt	Low-Ti basalt	0.124030	0.512646	7	0.2	3.8
KOP 1/10	Basalt	Low-Ti basalt	0.114363	0.512623	7	−0.3	3.9
KOP 1/11	Basalt	Low-Ti basalt	0.112858	0.512670	18	0.6	4.7
KOP 1/12	Basalt	Mid-Ti basalt	0.110555	0.512640	7	0.0	4.4
NVS 1/5	Basalt	Low-Ti basalt	0.111042	0.512634	9	−0.1	4.2
BAT 1/6	Continuous	Low-Ti basalt	0.133017	0.512662	6	0.5	3.7
BAT 4/11	Continuous	Low-Ti basalt	0.113764	0.512597	7	−0.8	3.4
BAT 4/13	Continuous	Low-Ti basalt	0.117009	0.512635	5	−0.1	4.0
BAT 3/5	Continuous	Mid-Ti basalt	0.117713	0.512663	4	0.5	4.5
BAT 3/23	Continuous	Mid-Ti basalt	0.123507	0.512691	7	1.0	4.7
BAT 1/8	Continuous	Trachyte	0.114467	0.512606	12	−0.6	3.5
BAT 4/2	Continuous	Trachydacites	0.109523	0.512598	10	−0.8	3.6
BAT 5/1	Continuous	Trachyandesite	0.117082	0.512608	7	−0.6	3.4
BAT 1/12	Continuous	Rhyolite	0.101176	0.512485	9	−3.0	1.8
BSK 1/5	Continuous	Rhyolite	0.114480	0.512503	6	−2.6	1.5
KHK 2/9	Bimodal	High-Ti basalt	0.119950	0.512832	8	3.8	7.7
KHK 1/2	Bimodal	High-Ti basalt	0.133784	0.512809	5	3.3	6.5
KHK 5/30	Bimodal	High-Ti basalt	0.131874	0.512784	11	2.8	6.1
KHK 10/3	Bimodal	High-Ti basalt	0.132352	0.512802	10	3.2	6.4
KHK 11/2	Bimodal	High-Ti basalt	0.124153	0.512770	5	2.6	6.2
KBU 3/12	Bimodal	High-Ti basalt	0.119853	0.512778	4	2.7	6.6

($TiO_2 \sim 1.05$–1.55 wt%) and mid-Ti ($TiO_2 \sim 1.58$–1.77 wt%). TiO_2 varies irrespective of the total alkalinity ($Na_2O + K_2O$) and SiO_2.

The basalts have phenocrysts of olivine, augite and labradorite. The groundmass has hyalopilitic or vitrophyre structure; it is composed of devitrified glass bearing visible fine grains of clinopyroxene, plagioclase, magnetite and apatite needles. Regarding the texture and mineral composition, trachybasalts and intermediate basaltic trachyandesite-phonotephrites are similar to the basalts. However, olivine is not present as phenocrysts. In addition, along with labradorite there appears andesine, sheets of pale biotite and prismatic crystals of

Fig. 9. Spider diagrams of Devonian magmatic rocks of the Altai-Sayan Rift System. Rocks associations: (a) Basalt. (b-d) Continuous. (f-g) Alkaline. (h-i) Bimodal. (j) Ultramafic – mafic. OIB = basalts of the oceanic islands (Sun and McDonough, 1989), IAB = island arc basalts (Kelemen et al., 2003), LTB Siberian Traps LIP = low-Ti ($TiO_2 \approx 1.01$ wt%) basalts (Al'mukhamedov et al., 2004), MTB Siberian Traps LIP = mid-Ti ($TiO_2 \approx 2.45$ wt%) basalts (Al'mukhamedov et al., 2004), HTB Siberian Trap LIP = high-Ti ($TiO_2 \approx 3.59$ wt%) basalts (Wooden et al., 1993), LC = lower of the continental crust (Rudnick and Gao, 2003), UC = upper of the continental crust (Rudnick and Gao, 2003). Data for Belogorsk alkaline intrusion (Vrublevsky et al., 2016), Mongolian peralkaline granites (Kovalenko et al., 2004b), Mongolian picrites and picrobasalts (Izokh et al., 2011). Diagrams emphasize the differences in the geochemical parameters of low-Ti, mid-Ti and high-Ti basalts indicating a combination of plume mantle component (OIB type) and subduction-modified lithospheric mantle component (IAB type) for sources of primary melts; SiO_2-rich rhyolites are depleted in incompatible elements suggesting anatectic melting of continental crust; and peralkaline granites-pantellerite are enriched in incompatible elements suggesting fractionation of high-Ti basalt melts.
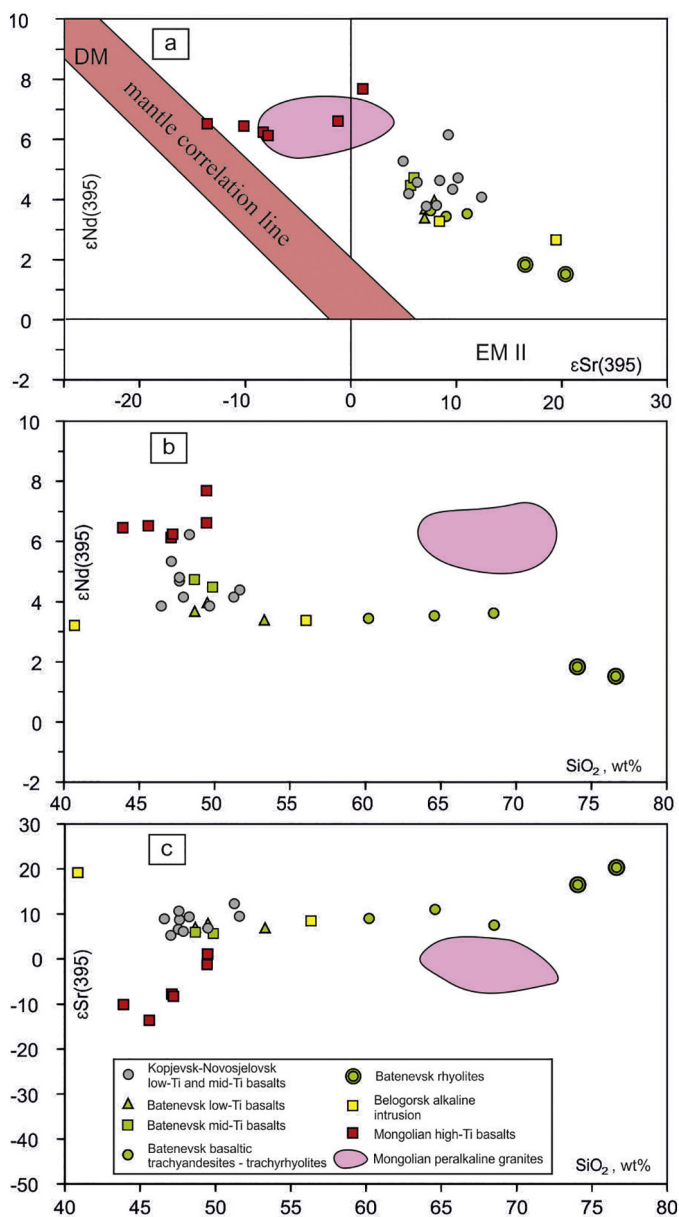
Fig. 10. Isotope classification of the Devonian magmatic rocks of the Altai-Sayan Rift System. Data for Belogorsk alkaline intrusion (Vrublevsky et al., 2016), Mongolian peralkaline granites (Kovalenko et al., 2004b). (a) εNd(395) vs. εSr(395) diagram. DM – depleted mantle component, EM II – enriched $^{87}Sr/^{86}Sr$ mantle components (Zindler and Hart, 1986). Mantle correlation line is recalculated to 395 Ma. Rock compositions are shifted from the mantle correlation line towards the radiogenic Sr-rich substrates suggesting the assimilation with the mantle melts of a crust component. (b) εNd(395) vs. SiO₂ (wt%) diagram. (c) εSr(395) vs. SiO₂ (wt%) diagram. Note increase in εSr(395) values and decrease in εNd(395) values for SiO₂-rich rhyolites supporting geochemical data for the addition of a contaminant to the products of low-Ti basalt magma differentiation.

common hornblende. All rocks have undergone post-magmatic alteration, to a varying extent. Chlorite-group minerals replace augite, serpentine develops after olivine, and talc, chlorite and secondary magnetite are also present.

5.1.2. Continuous association

The volcanic association of the Batenevsk outcrop consists of these rock groups: (1) basaltic: basalt, dolerite, trachybasalt and basaltic trachyandesites, (2) trachyandesite, (3) trachyte and trachydacite, and (4) trachyrhyodacite and rhyolite. On the TAS diagram, their compositions lie in the field of moderately alkaline rocks.

Rocks of mafic composition predominate. Values of Na₂O + K₂O ~ 3.4–4.6 wt% at SiO₂ ~ 47.7–53.3 wt% are characteristic for the basalts and dolerites. There are also trachybasalts and basaltic trachyandesites which have a higher content of Na₂O + K₂O (5–7 wt %) and similar SiO₂ (49.6–53.5 wt%). The mafic rocks are split into two groups by TiO₂ content: low-Ti (TiO₂ ~ 1.27–1.44 wt%) and mid-Ti (TiO₂ ~ 1.56–2.15 wt%).

Low-Ti basalts are present throughout the sequnce, while mid-Ti basalts occur only at the bottom (basalt-basaltic trachyandesites) and middle (basalt-trachyandesite-trachyte-trachydacite) portions of the sequence. Rocks of both subgroups share similar petrographic features.

Trachyandesites exhibit a porphyry-like texture, and typically have a trachytoid, in places glassy, texture. Phenocrysts include augite and zoned plagioclase (andesine in the core and oligoclase in the periphery), and sometimes K—Na feldspar with perthite structure. The groundmass consists of devitrified volcanic glass bearing very fine crystals of plagioclase, clinopyroxene and other chloritized dark minerals like amphibole, biotite and ore minerals. Compositions cover the range SiO₂ ~ 55–61 wt %, Na₂O + K₂O ~ 6.7–9.0 wt%.

Trachytes and trachydacites contain large (reaching 10 mm) phenocrysts of alkaline feldspar with a perthitic structure, micro phenocrysts of augite (in places hypersthene and diopside), and rarely quartz and plagioclase. Two types of zonation are observed in the plagioclase phenocrysts. One type consists of direct progressive zonation from andesine to oligoclase from core to rim. The other type of zoning is rhythmic with compositions varying back and forth between andesine and albite. In some volcanic varieties, the phenocrysts of alkaline feldspar show rounded shapes and diffuse edges, thus indicating reactionary relationships of crystals with melt. The groundmass consists of grains of irregularly shaped alkaline feldspars, altered dark minerals, microlites of acid plagioclase (An₁₀₋₁₂) and ore minerals, and in which minute interstices involve quartz and brownish devitrified glass reaching 5%. In trachytes, the amount of quartz is insignificant, while in trachydacites this mineral is common. The texture of the rocks is serial - porphyry-like, their dominant texture is hypidiomorphic granular, and in places the texture is trachytoid and glassy. SiO₂ abundance in rocks of this group varies within 62.5–64.5 wt%, Na₂O + K₂O ~ 7–10 wt%.

Primarily composed of quartz and alkaline feldspar the phenocrysts compose about 20% of the trachyrhyolites and rhyolites. At some sites, scarce oligoclase grains are present. These rocks typically show a porphyritic structure and fluidal texture. They have felsic, rarely micro spherulite structures and contain spots with micrographic intergrowths of quartz and alkaline feldspar in a glassy matrix. Some pyroclastic formations like tuff lava, welded tuffs and ignimbrite include glassy flattened fragments with specific notched edges (fiamme), rare chips of quartz and feldspar, as well as small ash particles of horn-like shape, irregularly distributed in glassy matrix. Fe oxides often replace dark minerals. The composition of rocks varies within the following ranges: SiO₂ ~ 67–76.6 wt% and Na₂O + K₂O ~ 7–10 wt%. Trachydacite and rhyolite occur as infrequent flows in the middle part of the section, but are dominant at the top of the section. In the trachyte, trachydacites, trachyrhyolite and rhyolite units the agpaitic coefficient is 0.95 (molecular ratio of Na₂O + K₂O)/Al₂O₃; Le Maitre et al., 1997, Maitre (ed. et al., 2002)

5.1.3. Alkaline association

The alkaline association includes volcanic nephelinite, tephrite, phonotephrite, tephriphonolite, phonolite, alkaline trachyte and a wide spectrum of their alkaline intrusive analogs such as ijolite, urtite, teralite, foyaite and nepheline syenite. On the TAS-diagram the compositions of volcanics at the Goryachegorsk plateau and intrusive plagioclase ijolite and foyaite units of the Belogorsk pluton have compositions with variations of Na₂O + K₂O from ~8.7–12.8 wt% and SiO₂ from ~41.2–62.4 wt% (Vrublevsky et al., 2016). A key feature of these rocks is that all rock-forming oxides vary widely in composition.

Thus, in mafic rocks with SiO_2 ~ 41.2–54.0 wt% the TiO_2 content ranges between 0.37 and 1.91 wt%.

The principal petrographic characteristic of these rocks is the presence of nepheline, aegirine, kersutite, barkevekite, alkaline hornblende along with albite, alkaline feldspar and accessory minerals. In some varieties, e.g. phenocrysts of nepheline range in size from 0.5 cm to 2 cm and comprise ~50% of the rock volume.

5.1.4. Bimodal association

In northwestern Mongolia, the bimodal association includes the following rocks: (1) basalts, trachybasalts and teshenites, and (2) trachyrhyolites, alkaline trachyrhyodacites, pantellerites and peralkaline granites, with rare-earth mineralization as well. Group 1 rocks are larger in volume than those of Group 2.

The rocks of mafic composition (in this bimodal association) have higher $Na_2O + K_2O$ (3.8–8.0 wt%) and much lower values of SiO_2 (43.9–49.5 wt%) than in rocks of the continuous association (Section 5.1.2). The basalts in the bimodal association also typically show a high abundance of TiO_2 (2.17–4.05 wt%), and have aphyric fine-grained and glassy textures. The main rock forming minerals are plagioclase, olivine and Ti-augite. In addition, there is apatite, platy biotite, regularly distributed ore and accessory minerals, and green-brownish volcanic glass filling interstices. The most alkaline varieties include xenomorphous nepheline or analcime, as well as fine crystals of kersutite and barkevekite. The same set of minerals is common for teshenites which have a hypidiomorphic-granular structure.

Trachyrhyolite and pantellerite rocks display a serial-porphyry texture. Phenocrysts consist of aggregates of crystals of tabular perthitic

K—Na feldspar. The groundmass is composed of oriented microliths of K—Na feldspar; in between there are amorphous crystals of quartz, fine grains of ore and accessory minerals, and microliths of arfvedsonite with distinct pleochroism from dark blue to greenish to light yellow-greenish. In these rocks, SiO_2 varies within 68–74 wt%, and $Na_2O + K_2O$ ~ 10.2–11.1 wt%. The agpaitic coefficient in trachyrhyolites varies from 0.92 to 1.00, and in pantellerites it is 1.00–1.25.

Rare-metal peralkaline granites of the Khaldzan-Buregtei massif have hypidiomorphic-granular or porphyry-like structure. In porphyritic varieties, phenocrysts comprise K—Na feldspar, quartz and arfvedsonite. The groundmass contains aggregates of arfvedsonite, aegerine, albite, quartz, fluorite, apatite and sphene. In these granites the "snow ball" structures represent albite overgrowth zones on grains of K—Na feldspar, and rarely on grains of quartz or arfvedsonite and reflecting simultaneous or close to simultaneous crystallization. Rare-metal – rare-earth mineralization is associated with zircon, elpidite $Na_2ZrSi_6O_{15} \cdot 3(H_2O)$, quartz-gittinsite pseudomorphs after elpidite, pyrochlore, rare-earth carbonate and polilithionite $KLi_2AlSi_4O_{10}F_2$. SiO_2 ranges within 70–72 wt%, $Na_2O + K_2O$ ~ 8.2–9.1 wt%. The agpaitic coefficient is 1.2 (Kovalenko et al., 1989).

5.2. Incompatible-element geochemical systematics

5.2.1. Basalt association

Mafic rocks of this association are similar to island arc basalts (IAB) based on their low contents of Nb and Ta relative to La (Ta/La)$_n$ ~ 0.33), and low Zr, Hf and Ti (Fig. 9a). This characteristic is evidence for melts derived from water-saturated mantle sources (Briqueu et al.,
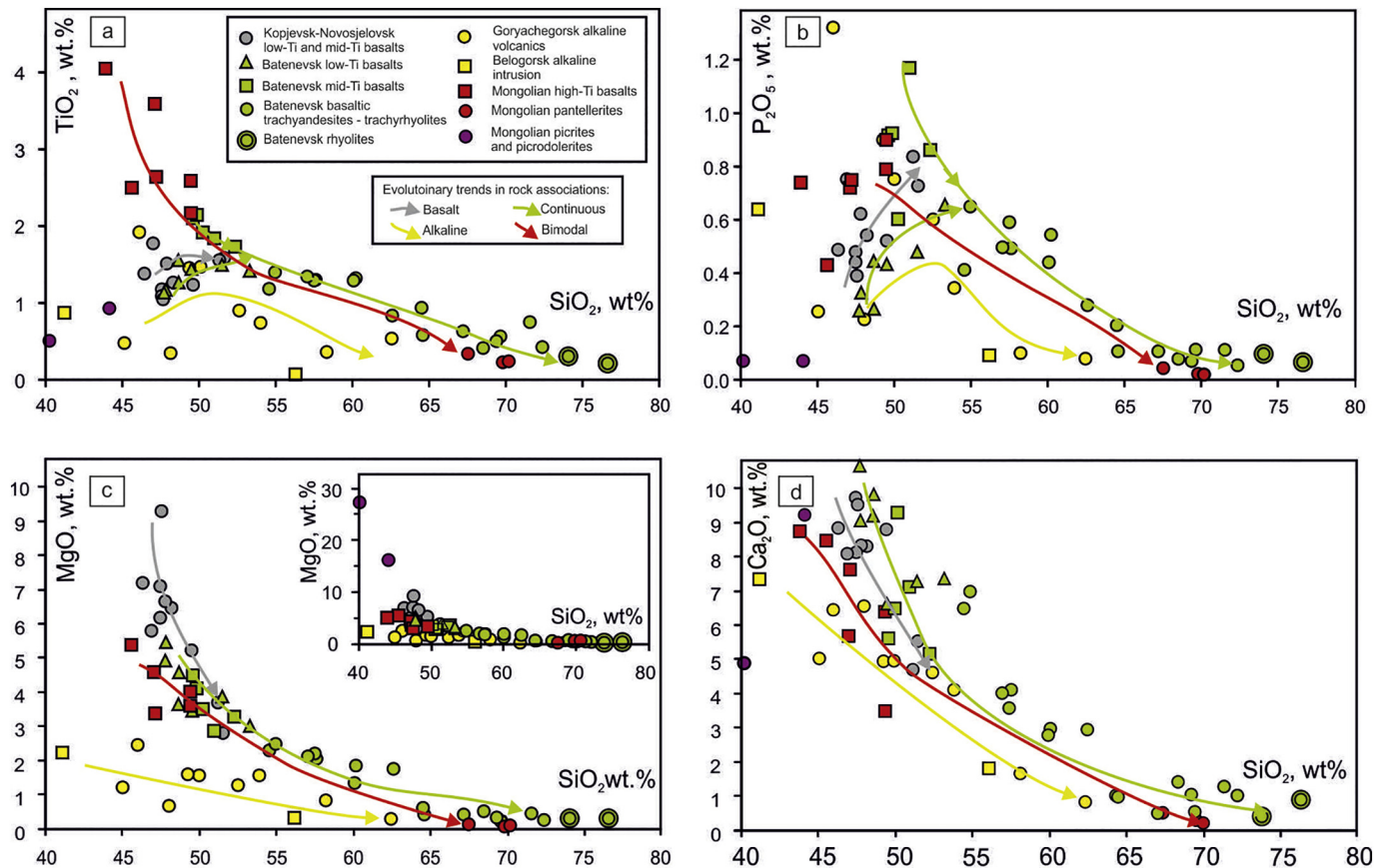
Fig. 11. (a-d) TiO_2, P_2O_5, MgO, CaO (wt%) vs. SiO_2 (wt%) content for Devonian magmatic associations of ASRS illustrating evolutionary trends of mineral crystallization. These plots show that variations of TiO_2, P_2O_5, MgO, and CaO are controlled by fractionation of Ti-magnetite, apatite, Mg-containing silicates and Ca-containing silicates in the trends of high-Ti basalts – pantellerites, mid-Ti basalts – rhyolites and trachyandesite – rhyolites. Low-Ti mafic melts changed their composition owing to fractionation of olivine and Ca-containing silicates in the trend of low-Ti basalts – trachyandesites.
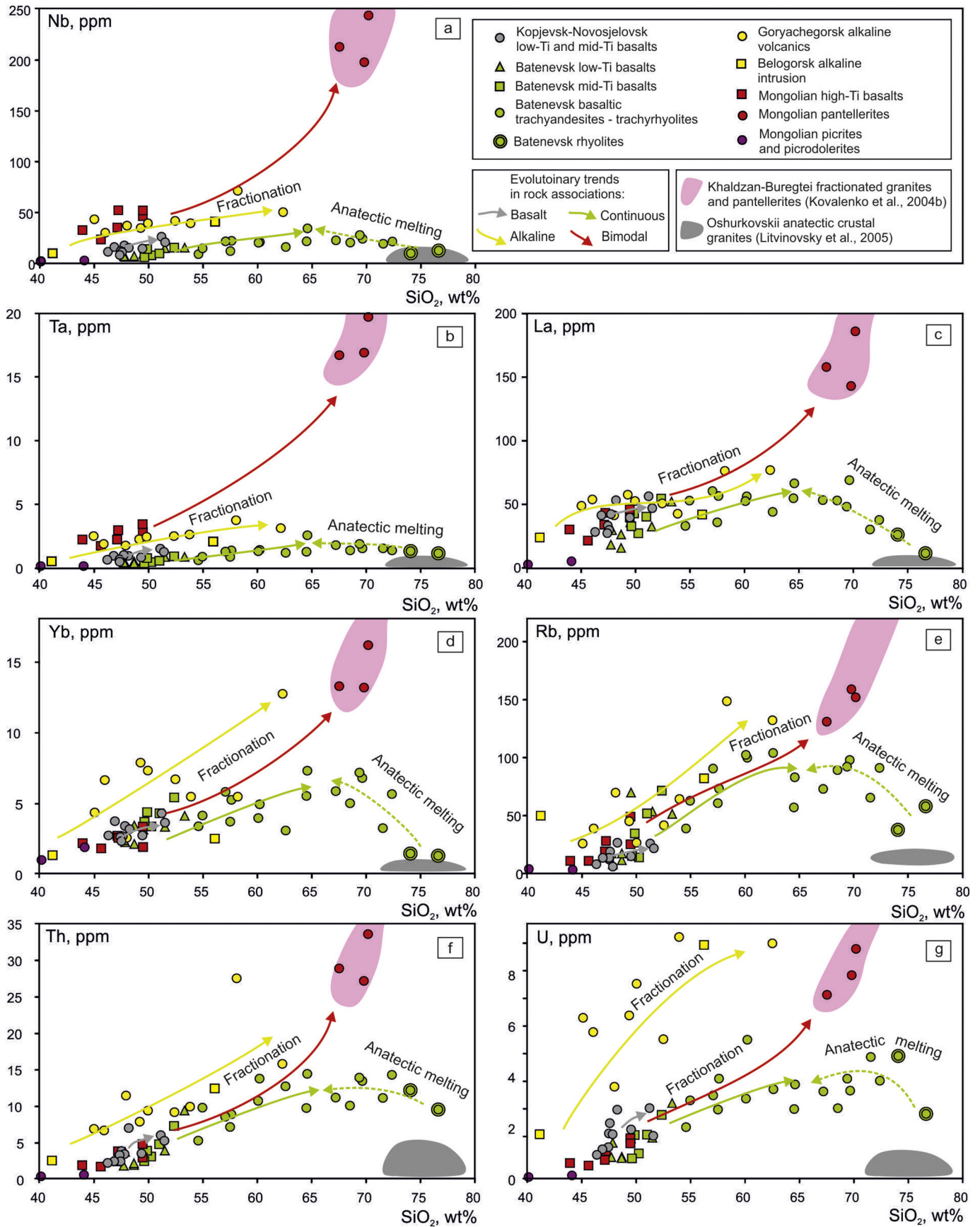
Fig. 12. (a-g) Nb, Ta, La, Yb, Rb, Th, U (ppm) vs. SiO$_2$ (wt%) diagrams for rocks of the Devonian magmatic associations of the Altai-Sayan Rift System. The chemical trends show direct correlation of these elements with SiO$_2$ in the series of high-Ti basalts – pantellerites, mid-low-Ti basalts – trachytes (65 wt%) indicating mineral fractionation of mantle melts; inverse correlation of these elements with SiO$_2$ in trachyte – rhyolite (77 wt%) series and illustrating the appearance in the magmatic system of anatectic crustal melts.
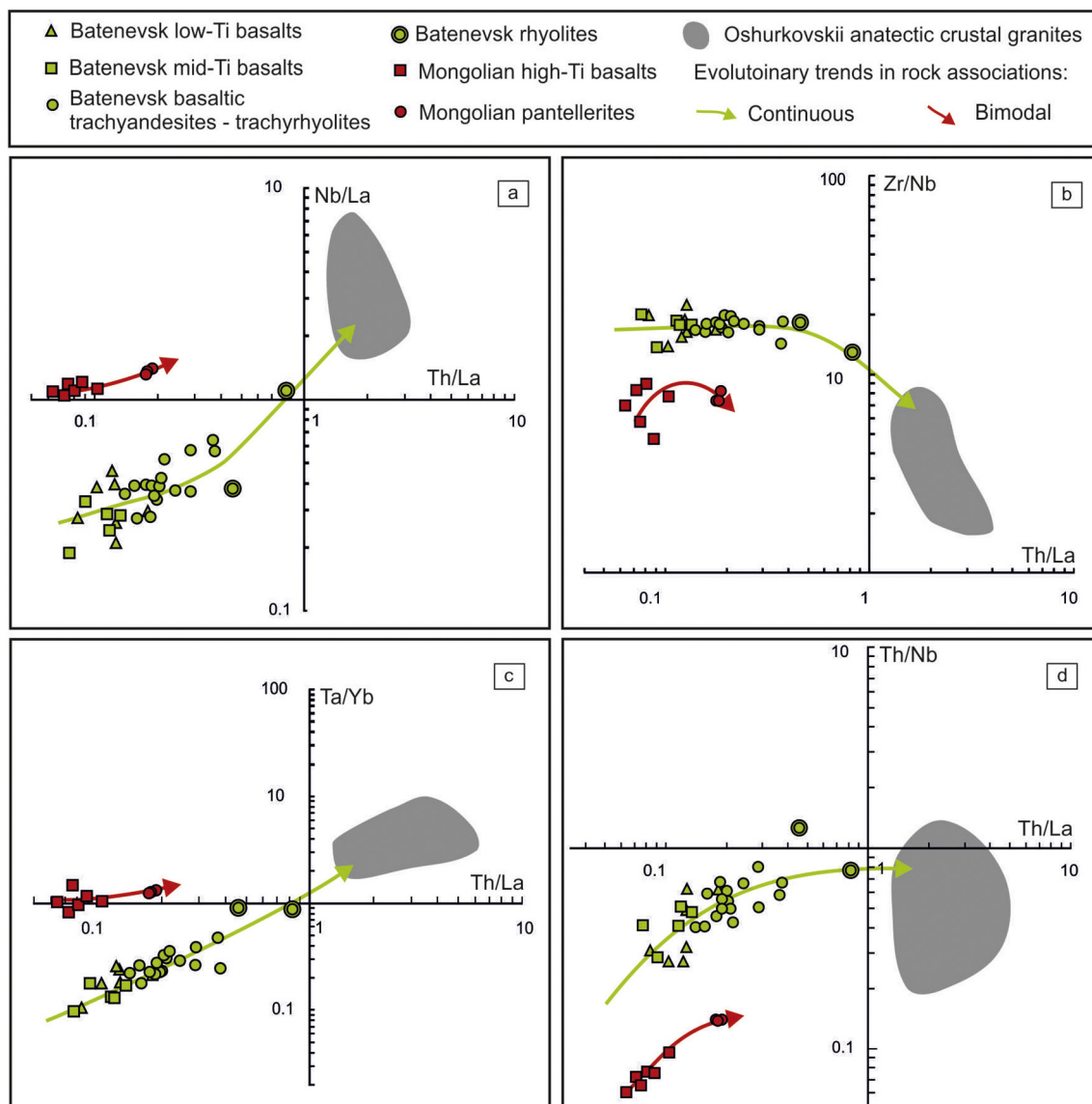
Fig. 13. (a-d) Th/La vs. Nb/La, Th/La vs. Zr/Nb, Th/La vs. Ta/Yb and Th/La vs. Th/Nb diagrams for rocks of the the Devonian continuous and bimodal associations of the Altai-Sayan Rift System. The data produce diverse trends indicating varying composition of sources and different mechanisms of their formation. The compositions of rocks of the continuous association define a long trend (green line) due to fractionation of basaltic magma resulting in the formation of trachyte melts. Low-alkaline high-Si rhyolites of continuous association deviate towards the anatectic granite-pegmatite (Litvinovsky et al., 2005), pointing to close compositions of their sources. The compositions of rocks of bimodal association define a short trend (red line), possibly due to fractionation of basalt melts.

1984; Hawkesworth et al., 1991, 1993; Ryerson and Watson, 1987; Pearce and Peate, 1995). However, in contrast to IAB, these rocks have higher abundances of all incompatible elements, and in this sense, they approach OIB, particularly in their REE distribution pattern. Their intermediate character between IAB and OIB makes it possible to compare these basalts with low-Ti basalts in the trap (LIP) provinces having similar geochemical features (Al'mukhamedov et al., 2004).

5.2.2. Continuous association

In this association, basaltic flows are compositionally similar to rocks of the basalt association (Section 5.2.1). They are also rich in rare lithophile elements; however, they possess a more distinct positive anomaly of Ba (Fig. 9b,c). In this case, we should underline the difference of geochemical parameters between low-Ti and mid-Ti basalts. The former are depleted in nearly all incompatible elements, except for Ba and Sr. At the same time, they are similar in the pattern of REE

differentiation (La/Yb)$_n$ ~ 6 for low-Ti basalts, (La/Yb)$_n$ ~ 7 for mid-Ti basalts.

In comparison to the basalts, the other units of the continuous series, basaltic trachyandesites, trachyandesites and trachytes (Fig. 9d) and trachydacites-trachyrhyolites (Fig. 9e), show an increase in Rb, Th, U, Nb, Ta, Zr, Hf, a negative Nb—Ta anomaly, and negative anomalies of Sr, P and Ti.

Rhyolites of continuous association (SiO$_2$ > 74 wt%) are depleted in incompatible elements. In this respect, they are close to the average composition of the upper continental crust (Fig. 9e) from which they differ by having much lower contents of P, Ti and HREE. In comparison with them the trachyrhyodacites (SiO$_2$ ~ 65–74 wt%) are enriched in nearly the entire spectrum of incompatible elements. As regards geochemical features, they are similar to trachytes, and only distinguished by lower P and Ti. Their compositions are not fractionated in the HREE nor in the MREE areas.

5.2.3. Alkaline association

The rocks with SiO_2 ~ 41–54 wt%, volcanic nephelinites, tephrites, phonotephrites and tephrophonolites, show some differences with basalts of the other ASRS associations. Considering Nb, Ta, LREE and MREE contents, they belong to the OIB type (Fig. 9f). The Nb—Ta minimum (negative anomaly) is small and unimpressive. At the same time, these rocks have anomalously high contents of Rb, Ba, Th, U, Sr and HREE exceeding those in OIB. They are however impoverished in Ti and are close in TiO_2 to basalts of low-Ti group of ASRS. As compared to mafic alkaline volcanics, the plagioclase ijolites of the Belogorsk pluton (Vrublevsky et al., 2016) are poor in incompatible elements, except for Rb, Sr, P and U.

In volcanic phonolites and alkaline trachytes (SiO_2 ~ 54–63 wt%) the concentrations of incompatible elements increase (Fig. 9g) in comparison with the rocks with SiO_2 ~ 41–54 wt%. The HSFE and REE abundances considerably exceed those in the rocks of the upper continental crust. Low Ba, Sr, P and Ti typify alkaline volcanics. Foyaites of the Belogorsk pluton are similar in composition to phonolites and alkaline trachytes, but are distinguished by higher Ba, and lower Ti, Zr, Hf, MREE and HREE.

5.2.4. Bimodal association

In northwestern Mongolia, high-Ti basalts of bimodal association are rich in LREE (($La/Yb)_n$ ~ 11) and HSFE, and haveweak positive anomalies in Nb and Ta (($Nb/La)_n$ ~ 1.05, ($Ta/La)_n$ ~ 1.16), and are similar in composition to OIB (Fig. 9h). In pantellerites and peralkaline granites (SiO_2 ~ 68–70 wt%), the contents of rare lithophile elements, except for Ba, Sr, P and Ti are noticeably in excess of those in crustal rocks (Fig. 9i). In these rocks, in contrast to continuous association, there is a distinct negative Eu anomaly (($Eu/Eu^*)_n$ ~ 0.15), which indicates a marked input of fractionation to their formation.

5.3. Sr and Nd isotopes

Twenty-six samples of volcanic rocks have been analyzed for isotope composition of Sr, Nd, and results are listed in Tables 2 and 3. These samples are distributed among the associations as follows: basalt - 10, continuous - 10, bimodal - 6. These are augmented by literature data for rocks of the alkaline association (Vrublevsky et al., 2016) and granites of the bimodal association (Kovalenko et al., 2004b).

Sr and Nd isotopic data confirm the differences for each association revealed from geochemical data. Thus, all rocks of the basalt and continuous associations (Fig. 10a-c) are rich in radiogenic Sr (εSr (395) > 5.1) and depleted in radiogenic Nd (εNd(395) < 6.2) in comparison with rocks of the bimodal association. In the continuous association the mid-Ti basalts are more depleted in Sr composition (εSr (395) ~ 5.7–6.0) against low-Ti basalts (εSr (395) ~ 7.0–8.0). High-Ti basalts are distinguished by much lower radiogenic Sr (εSr (395) ~ (−13.6)–1.2) but retain the tendency to be enriched with radiogenic Nd (εNd (395) ~ 6.1–7.7).

6. Discussion

6.1. Magmatic sources and diverse Ti-types of LIP-basalts

Geological and mineralogical signatures of magmatic rocks in ASRS (Altay-Sayan LIP; Kuzmin et al., 2010; Kravchinsky, 2012; Ernst et al., 2020) are broadly similar to other complexes of LIP in accordance with the criteria proposed by Bryan and Ernst (2008) and Ernst (2014). The magmatic rocks in the ASRS (also Altay-Sayan LIP) consist of voluminous mafic magmatism including picrites centred on a triple junction rift system but also distributed over a broader region. Geochemical features of basic rocks in the ASRS typify basalts of LIPs, which include varieties with both high-Ti and low-Ti abundances (Ernst, 2014). Such basalts occur in many provinces, e.g. Siberian Traps LIP (Al'mukhamedov et al., 2004; Wooden et al., 1993; Ivanov

et al., 2013), Karoo LIP of South Africa (Neumann et al., 2011; Jourdan et al., 2007) and Emeishan LIP in southern China and Vietnam (Xu et al., 2004). Some LIP basalts may be close to OIB composition at high contents of TiO_2, ($Nb/La)_{pm}$ and ($Ta/La)_{pm}$. Such basalts are comparable with magmas of mantle plumes (Campbell, 2001; Ernst et al., 2005; Condie, 2001; Kieffer et al., 2004; Saunders et al., 1992; Xia, 2014; Xia and Li, 2019). Other LIP basalts have low abundances of TiO_2 (Wilson, 1989), Nb and Ta (Thompson et al., 1984). They are related either with the products of melting of lithosphere or hydrated mantle, or with contamination of mantle melts with crustal components (Wood, 1980; Saunders et al., 1992; Kieffer et al., 2004; Xia et al., 2008).

This range in the composition of mafic rocks also occurs in the volcanic associations of the ASRS. There are also intermediate and felsic rocks present and their formation is linked with contamination of primary melts with the upper crust material and via melt fractionation.

6.2. Magma evolution

Low-Ti (TiO_2 ~ 1.27–1.56 wt%) and mid-Ti (TiO_2 ~ 1.73–2.15 wt%) basalts of ASRS (Fig. 9a–f) are analogous to the basalt groups of the Siberian Traps LIP with TiO_2 ~ 1.01–2.45 wt% (Al'mukhamedov et al., 2004). In this connection, the ASRS might display some characteristics of mafic melt evolution, which gave rise to formation of both the continuous and alkaline associations. They (Fig. 11a–d) share a common pattern for compositional evolution in low-Ti basalts.

The mid-Ti basalts evidently evolved during a time of fractionation of Ti-magnetite, apatite, olivine and Ca-containing silicates, that agrees with the data on their petrographic composition and with variations of petrogenic elements (increase of SiO_2 from 49.6 to 54 wt%, decrease of TiO_2 from 2.15 to 1.56 wt%, and reduction of P_2O_5, MgO, and CaO). Low-Ti basalts of basalt and continuous associations modified their composition due to fractionation only of olivine and Ca-containing silicate that caused a sharp drop of MgO and CaO contents. In the continuous association, the change of compositions from trachyandesite (about 55.5 wt% SiO_2) to trachyte (64.5 wt% SiO_2) was apparently due to fractionation of Ti-magnetite, apatite, Mg-containing silicates, Ca-containing silicates and accumulation of feldspar in residual melts following Bowen's (Bowen, 1928) trend of mineral crystallization. In the
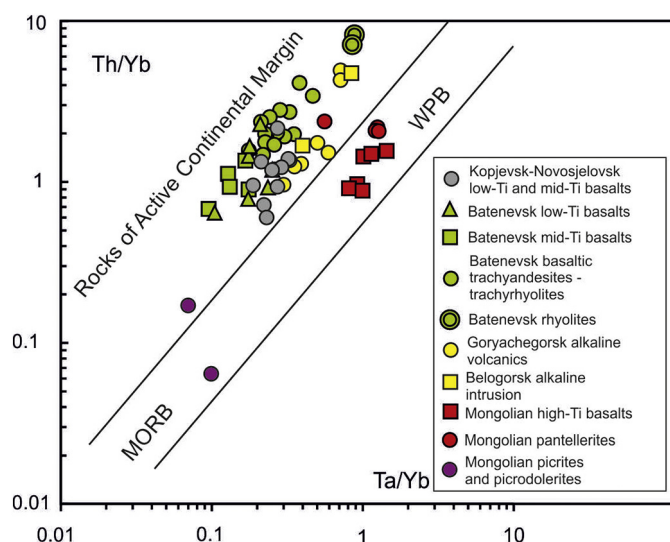

Fig. 14. Tectonic discriminant diagram Th/Yb vs. Ta/Yb (Pearce, 1982) illustrating that: 1) the basalt, continuous and alkaline associations belong to compositional field of the active continental magin-related series; 2) the ultramafic-mafic association predominantly belongs to compositional field of the mantle depleted (mid-oceanic ridge basalts type); and 3) the bimodal association belongs to the compositional field of the within-plate series. MORB = Mid-Oceanic Ridge Basalts, WPB = Within-Plate Basalts.

line of compositions from trachytes to rhyolites, there appear rocks with anomalously low contents of TiO_2, P_2O_5, MgO, and CaO. Therefore, we infer, that felsic volcanics of the continuous association have their own pattern of development, which distinguishes them from the products of progressive differentiation of basalt magmas.

On the plots in Fig. 12a–g, the basalt-trachyte trend of the continuous association exhibits a direct correlation between the contents of incompatible elements (Zr, Nb, Ta, La, Yb, Rb, Th, U) and increase in SiO_2 values; it is changed in trachytes at SiO_2 values of about 63–65 wt%.

Trachydacites and rhyolites demonstrate different geochemical behavior, showing inverse ratios between REE and SiO_2 contents. The REE growth starts from rhyolites compositionally similar to the anatectic crustal granites exemplified by granite-pegmatites of the Oshurkovskii massif of the western Trans-Baikal region (Litvinovsky et al., 2005). It is notable that the marginal zone between the two different trends (SiO_2 ~ 65 wt%) displays the broadest scatter of contents of both petrogenic and incompatible elements..

Importantly, the behavior of pairs of incompatible elements reflects crustal contamination during formation of felsic rocks of the continuous association (Fig. 13). On this plot, there are linear trends between trachydacites and anatectic granite-pegmatites of the Oshurkovskii massif. On the plots Th/La vs. Nb/La, Th/La vs. Zr/Nb, Th/La vs. Ta/Yb and Th/La vs. Th/Nb, the trends bend at the boundary between trachytes and rhyolites. Fractionation along the basalt-trachyte trend contributed to a moderate enrichment of rocks with Th, Nb and Ta. The appearance of low-alkaline high-Si rhyolites was accompanied by the deviation of compositions towards anatectic granite-pegmatites (Litvinovsky et al., 2005), pointing to close compositions of their sources. The plots also illustrate the compositional variations of rocks of the bimodal magmatic association. Basalts to pantellerites demonstrate a different trend, indicating that crust contamination never affected rocks of this association.

The compositional data for the basalt association of the Kopjevsk and Novosjelovsk areas (Figs. 11a–d and 12a–g) links to beginning of the modified composition trend for low-Ti basalts of the continuous association. This indicates both associations being linked to the same magmatic source.

Compared to the continuous association, the rocks of the bimodal magmatic association display a break in composition between high-Ti (TiO_2 ~ 2.17–4.05 wt%) basalts and associated pantellerites and peralkaline granites. The high-Ti basalt compositions of bimodal magmatic association evolved through differentiation of mid-Ti basalts of continuous association. Primitive compositions represent mostly low-Si (SiO_2 = 43.9 wt%) and high-Ti (TiO_2 = 4.05 wt%) varieties. With increasing SiO_2 the TiO_2, P_2O_5, MgO, and CaO abundances noticeably decrease, suggesting fractionation of Ti-magnetite, apatite, Mg-containing silicates and Ca-containing silicate (Fig. 11a–d). Felsic rocks, e.g. trachyrhyolites and pantellerites, are separated from mafic rocks by a gap at intermediate composition, but geochemical and isotope data demonstrate a genetic relationship between mafic and felsic rocks. High-Ti basalts of this association are enriched in Zr, Nb, Ta and La of mid-Ti and low-Ti basalts of the Batenevsk area. High-Ti basalts (Fig. 9h) share affinity with the basalts of the Siberian Trap LIP (high-Ti basalts (TiO_2 = 3.59 wt%; Wooden et al., 1993). Their compositions begin the trend (solid line) of an increase in incompatible element abundance (Fig. 12a–g) along the entire range of SiO_2 featuring magmatic differentiation and the appearance of residual pantellerite-peralkaline granite melts with anomalously high contents of rare lithophile elements.

Complicated relationships are typical for rocks of the alkaline association. They have low contents of MgO pointing to a high degree of initial fractionation from mantle melts. Considering their petrogenic evolution they resemble the rocks of basaltic and continuous associations (Fig. 11a–d). At the same time, volcanic rocks (SiO_2 ~ 45–54 wt%) have anomalously high U, Sr, HREE (Fig. 9f), and they show growth of incompatible elements with increasing SiO_2 (Fig. 12a–g). High values

of Rb, Th and U contents are analogous to those in pantellerites-peralkaline granites.

In northwestern Mongolia, the compositions of picrites and picrodolerites lie at the beginning of the trend for low-Ti mafic rocks (Fig. 11a,c). These rocks are poor in TiO_2, P_2O_5, and incompatible elements. Picrites with high MgO display a weak positive anomaly of Sr, slight depletion in U and Th, and the lowest concentrations of REE (Fig. 9j). Izokh et al. (2011) inferred that the composition of these rocks indicated their cumulative nature.

On the geochemical diagram Th/Yb vs. Ta/Yb (Fig. 14; Pearce, 1982), the compositions of both low-Ti and mid-Ti basalts have negative Ta anomalies similar to that exhibited by active continental margin magmatism and that effect is plausibly due to contamination of melts with lithospheric material. The bimodal associations with high-Ti basalts exhibit the features of a mantle plume without contamination processes involved.
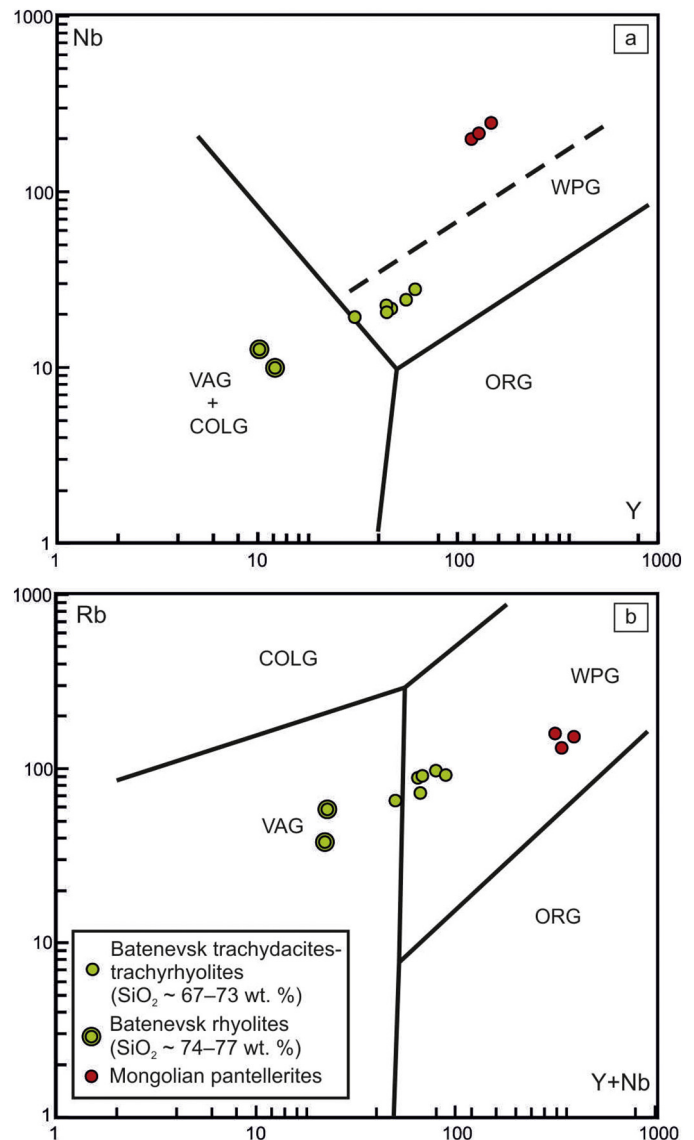

Fig. 15. (a-b)Tectonic discriminant diagrams Nb vs. Y and Rb vs. Y + Nb (ppm) (Pearce et al., 1984) for felsic rocks of the Devonian continuous and bimodal associations of the Altai-Sayan Rift System. These diagrams show that the trachydacites-trachyrhyolites and pantellerites are most related to within-plate series, and that the high-Si low-alkaline rhyolites belong to compositional field of the arc-related, collisional-related series. COLG = collisional granites, WPG = within-plate granites, ORG = ocean ridge granites, VAG = volcanic arc granites.

Similar geochemical patterns apply to the felsic rocks. Thus, on the Nb vs. Y and Rb vs. Y + Nb tectonic discrimination diagrams (Fig. 15; Pearce et al., 1984), the trachydacites-trachyrhyolites (SiO_2 from 69 to 72 wt%) of the continuous association are transitional between arc-, collision-related and within-plate settings. However, low-alkaline high-Si rhyolites (SiO_2 from 74 to 77 wt%) have volcanic-arc and collisional affinities. Pantellerites (SiO_2 from 68 to 71 wt%) of the bimodal association plot in the within-plate fields.

These lines of evidence indicate that the composition of mantle sources of rocks of basaltic, continuous, alkaline and bimodal associations were heterogeneous. Its products were basalts with low, middle and high TiO_2 abundances and varying concentrations of incompatible elements. Their evolution resulted in formation of basalts with diverse TiO_2 contents and variable abundances of incompatible elements.

In all the associations, isotope (Sr, Nd) compositions of mafic rocks (Fig. 10a) shifted from the line of mantle correlation towards the crustal substrates rich in radiogenic strontium. Such a deviation apparently reflects assimilation by mantle melts of a component with high Sr, increased value $^{87}Sr/^{86}Sr$ and low REE abundances. These criteria could fit carbonate rocks, which subducted into the mantle in the Early Paleozoic. Their input into the mantle source areas could result in melts enriched in radiogenic strontium. The largest deviation of isotope compositions of magmatic sources from the trend of mantle correlation is observed in mid-Ti and low-Ti basalts of the basaltic, continuous and alkaline associations. This pattern is marked by the appearance of subduction geochemical signatures, e.g. reduced Nb and Ta contents (negative anomalies). High-Ti basalts of the bimodal association that deviate the least from the line of mantle correlation, thus suggesting less voluminous contamination of high-Ti melts.

In the continuous association, trachytes and rhyodacites are similar in isotope parameters to the low-Ti basalts. In rhyolites with low abundances of rare lithophile elements, $\varepsilon Sr(395)$ increases to 20.6 (Fig. 10b) along with a slight decrease in $\varepsilon Nd(395)$ from 1.8 to 1.5 (Fig. 10c); these trends are consistent with the interpretation of the role of crustal components being added to the basalt magma.

In contrast, the peralkaline granitoids of the Khaldzan-Buregtei massif, which is also part of the bimodal association, show quite different characteristics. The isotope composition of neodymium expressed through $\varepsilon Nd(395)$ varies from 4.4 to 8.7 which indicates moderately depleted to profoundly depleted mantle (Kovalenko et al., 2004b). By their isotope parameters, they correspond to the composition of high-Ti basalts, and a common mantle source. In particular, this demonstrates the leading role of fractionation differentiaton of parental mafic magmas to produce alkaline-granitoid melts.

6.3. Plume-lithosphere interactions

Considering the geological setting in that part of the Siberian paleocontinent, which was remote from any convergent boundaries, the ASRS appears to have an intraplate nature. As discussed above, the presence of a triple rift junction of sizable graben-like troughs and additional widespread grabens and troughs surrounding this junction, as well as the voluminous basaltic magmatism (with the charactreristics of a LIP), indicate that a mantle plume controlled magmatic and tectonic characteristics of this region.

6.3.1. Comparison with the late Cenozoic magmatic province of East Asia

The conflicting evidence for the geodynamic setting of the ASRS can potentially be understud through a comparison with the Late Cenozoic magmatic province of East Asia (Yarmolyuk et al., 1996, 2011a, 2015). The latter includes island arc systems on the border with the Pacific Ocean, rift structures along the continent margin and separate volcanic areas scattered over a huge area from the Japan arc and into northeast China reaching the Altai ranges. The Late Cenozoic magmatic province started in the Late Cenozoic about 30 Ma ago (Yarmolyuk et al., 2011a) and preceded the tectono-magmatic activity which commenced

on the continental margin about 20 Ma ago that accompanied the opening of the Sea of Japan.

This broad region include volcanics with both continental margin and within-continent (within-plate) geochemical signatures (Martynov, 1999; Hanyu et al., 2006; Lee et al., 2011; Yoshida et al., 2014; Hoang and Uto, 2003). Formation of this province can be interpreted in two ways. According to some the magmatism in the marginal part of the continent is mainly linked with subduction-related processes (Wang et al., 2011; Sakuyama et al., 2013; Chen et al., 2015), in particular, with the interaction of asthenosphere and lithosphere mantle (Hoang and Uto, 2003) or back-arc mantle upwelling (Chen et al., 2017). However, there are also magmas with a within plate singature and showing geochemical and isotopes signatures similar to OIB-type basalts (Yarmolyuk et al., 2011a, 2015).

Basic rocks of the Late Mesozoic - Cenozoic within-plate volcanic areas of Central Asia demontrate such characteristics. In the Early Cretaceous, they produced basalts showing pronounced Ta-Nb minimum (negative anomalies) irrespective of the level of enrichment with incompatible elements. In the end of the Early Cretaceous, this feature gradually decreased, and in the very end of Early- beginning of Late Cretaceous the basic rocks acquired the Ta-Nb maxima (positive anomaly) and full similarity to the OIB-type basalts. Such variability of compositions of basic rocks was caused by the impact of mantle plumes on the metasomatised mantle (Yarmolyuk et al., 1998, 2015, 2019). While magmatism developed in those areas, the metasomatized component was digested by the ascending mantle and but later ascending melts were not affected by metasomatized mantle.

The age differences, as well as remoteness of some within-plate areas from the subduction zone (up to over 3,000 km away from the subduction zone), allows formulation of the following interpretation, that the Late Cenozoic volcanic province in the east of Asia was formed in the area of interaction of the mantle hot field (mantle plume?) and convergent boundary. This point is verified by low-velocity seismic anomalies recorded at least in the uppermost part of the lower mantle in the basement of some of the volcanic areas (Hangai, South Baikal and Hainan) (Chen et al., 2015; Mordvinova et al., 2015). This model is relevant to the interpreting the ASRS magmatism. However, there is a difference. In the case of the Late Cenozoic magmatism of East Asia, subduction was coeval with the "hot mantle field", the plume-related magmatism. But, in the case of the Altay-Sayan event the Early Paleozoic subduction event that caused mantle metasomatism was much earlier than the plume-related magmatism of the ASRS.

6.3.2. Model of combined effects of plume and subduction

The evident similarity in the general structure of magmatic province of East Asia and Devonian volcanic province of the Altai-Sayan area suggests a similar scenatio of formation for the latter. We assume, that the rift part of the province (ASRS) originated above a large mantle plume, and so magmatism acquired some features similar to LIPs. As discussed above, the magmatic associations of the ASRS largely include the products of mafic magmatism, which are similar to LIP basalts (Cox et al., 1967; Marsh et al., 2001; Jourdan et al., 2007; Bryan and Ernst, 2008) and similarly vary in the contents of TiO_2 and incompatible elements. In addition, like in the LIPs, their varieties are distributed over a large area indicating heterogeneity of mantle sources involved in the formation of the ASRS.

It is now interpreted, that the low-Ti type of the LIP basalt magmas indicates contamination with subcontinental lithosphere or continental crust (Carlson, 1991; Peate, 1997; Ewart et al., 1998, 2004a, 2004b), and high degree of partial melting of the upper mantle or melting at low depths (Arndt et al., 1993; Xu et al., 2004). In contrast to that, the high-Ti mafic series of LIPs normally shows geochemical and isotope affinity to the OIB intraplate basalts, and these magmas are explained by melting of uncontaminated asthenosphere mantle or a plume component (Arndt et al., 1993; Zhao et al., 1994; Ewart et al., 1998, 2004a, 2004b). At the same time, basalts of continental LIPs are quite diverse

(Puffer, 2001); in places, they have a negative Nb—Ta anomaly, which might indicate melt interaction with metasomatized lithosphere mantle that had been earlier modified by subduction processes.

The continuous magmatic association displays geochemical features similar to low-Ti basalts of LIP provinces, and like the Parana-Etendeka and many other LIPs, they occur along with felsic magmatism resulting from crustal anatexis (Peate et al., 1992; Hawkesworth et al., 2000; Bryan et al., 2010; Ernst, 2014). Mafic rocks of the bimodal association can be compared with high-Ti basalts of LIPs with an assumed plume source of OIB type (Ernst, 2014).

The geochemical features of ASRS magmatism indicate interaction of magmatic sources of plume and supra-subduction origin. The ASRS is located in a fold belt, which emerged in the end of Cambrian-beginning of Ordovician by accretion of island arc complexes to the margin of the Siberian continent. Accretion proceeded along with subduction phenomena marked within the Altai-Sayan fold belt by numerous Early Paleozoic granitoid complexes (Rudnev et al., 2013). These facts reflect that accretion was followed by metasomatic processing of lithosphere mantle with water-fluid involved (Scambelluri and Philippot, 2001). Involvement of this mantle affected the composition of melting products (Humphreys and Niu, 2009; Till et al., 2011). With this evidence in mind, formation of magmatic associations of the Altay-Sayan Rift System/LIP is interpreted as follows.

In the period when magmatic associations started to form in ASRS, mantle plume magmas interacted with regional lithospheric mantle, which was metasomatically modified and enriched with water during the earlier Early Paleozoic (Caledonian) accretion and subduction events. Melting of such lithosphere mantle produced magmas similar in composition to those derived in subduction systems. This interpretation applies to the basalt magmas with low-Ti content and these melt products combined with the mantle plume magma providing two types of melts distinguished by their evolution pattern, e.g. moderately alkaline and alkaline. The moderately alkaline magmas arrived onto the surface, and in addition to that, the magmas of this type also remained in crustal chambers. This is where melts differentiated to trachyte compositions with insignificant contamination from host crustal material. Concurrently, partial melting of host rocks occurred in other magma chambers resulting in formation of anatectic crust melts under the thermal and magmatic impact of basaltic and differentiated magmas. This process resulted in low-alkaline rhyolite magmas with low abundances of incompatible elements, and which are poorer in radiogenic Nd, but richer in radiogenic Sr than basaltic melts. The end products of their evolution are similar to the composition of crustal melts.

After exhaustion of initial basaltic magmas in peripheral chambers the anatectic melts reached the surface as large extrusive sequences that marked the termination of the continuous volcanic association. Alkaline magmas forming the continuous nephelinite-tephrite-phonotephrite-phonolite association minimally interacted with crustal rocks.

The high-Ti magmas which were responsible for generation of bimodal magmatic association with peralkaline rare-metal granites, required maximal input from a mantle plume. The geochemical similarity of these basalts to OIB provide support for this interpretation. The felsic derivatives of such melts are rich in rare-lithophile elements, and they are similar to high-Ti basalt magmas with respect to the isotope parameters of Sr and Nd. This evidence suggests their formation in short-lived intermediate-depth crustal chambers via fractionation without a significant input of continental crustal material.

7. Conclusions

Newly acquired geological and isotope-geochemical data coupled with the results of preceding observations on the Devonan magmatism of the Altai-Sayan Rift System (also known as the Altai-Sayan LIP) indicate the following:

(1) Five magmatic associations are recognized: basalt, continuous, bimodal, alkaline and mafic-ultramafic. Mafic rocks exhibit a wide variation of TiO_2 (from 1.05 to 4.05 wt%) and are compositionally intermediate between intraplate basalts of OIB type and basalts of active continental margins of IAB type.

(2) The ASRS originated through a single magmatic pulse within the time interval 407–392 Ma in the southwestern framing of the Siberian Platform in a region that was composed of juvenile crustal complexes of Early Paleozoic age.

(3) The ASRS was derived independently of the convergence/subduction processes affecting the paleocontinent margin during the Middle Devonian.

(4) The composition of some ASRS magmatism was controlled by the lithosphere mantle being metasomatized during the prior Caledonian accretion and subduction events.

(5) The ASRS structure involves various magmatic associations, with the diversity of compositions defined by the varying extent and character of crust-mantle interaction. The composition and their diversity are interpreted as primarily controlled by a mantle plume with subduction-like magmatic associations derived from interaction with pre-Devonian metasomatized lithosphere. In addition, some more differentiated magmas originated through partial melting of lower mafic crust and some experienced differentiation and assimilation in mid-crustal chambers. This range of compositional variations are similar to those in many other LIPs.

CRediT authorship contribution statement

Declaration of competing interest

The authors declare that they have no known competing financial interests or personal relationships that could have appeared to influence the work reported in this paper.

Acknowledgements

References

Afonin, V.P., Gunicheva, T.N., Piskunova, L.F., 1984. X-Ray Fluorescence Silicate Analysis. Nauka Publishing House, Novosibirsk 228 p. (in Russian).

Al'mukhamedov, A.I., Medvedev, A.Ya., Zolotukhin, V.V., 2004. Chemical evolution of the Permo-Triassic basalts of the Siberian platform in space and time. Petrology 12 (4), 297–311.

Ananiev, A.R., 1959. Most Important Locations of the Devonian Floras in the Sayano-Altai Mountain Region. Tomsk State University Publishing House, Tomsk 99 p. (in Russian).

Arndt, N.T., Czamanske, G.K., Wooden, J.L., Fedorenko, V.A., 1993. Mantle and crustal contributions to continental flood volcanism. Tectonophysics 223, 39–52.

Ayalew, D., Gibson, S.A., 2009. Head-to-tail transition of the mantle: geochemical evidence from a Miocene bimodal basalt-rhyolite succession in the Ethiopian large Igneous Province. Lithos 112, 461–476.

Babin, G.A., Vladimirov, A.G., Kruk, N.N., Gibsher, A.S., Sovetov, Yu.K., Sergeev, S.A., Sennikov, N.V., 2004. Age of the initiation of Minua basins, Southern Siberia. Dokl. Earth Sci. 395 (3), 307–310.

Belyakov, N.A., Bulvanker, E.Z., Dubatolov, V.N., Eltysheva, R.S., Krishtofovich, A.N., 1955. In: Rzhonsnitskaya, M.A., Meleschenko, V.S. (Eds.), Field Atlas of Fauna and Flora of the Devonian Sediments of the Minusinsk Depression. Gosgeoltekhizdat Publishing House, Moscow 140 p. (in Russian).

Berzin, N.A., Kungurtsev, L.V., 1996. Geodynamic interpretation of geological complexes of the Altai-Sayan region. Russ. Geol. Geophys. 37 (1), 63–81.

Bowen, N.L., 1928. The Evolution of the Igneous Rocks. Princeton University Press, New Jersey 334 p.

Briqueu, I., Bongault, H., Joron, J.-L., 1984. Quantification of Nb, Ta, Ti and V anomalies in magmas associated with subduction zones: petrogenetic implications. Earth Planet. Sci. Lett. 68, 297–308.

Broussolle, A., Aguilar, C., Sun, M., Schulmann, K., Štípská, P., Jiang, Y., Yu, Y., Xiao, W., Wang, S., Míková, J., 2018. Polycyclic Palaeozoic evolution of accretionary orogenic wedge in the southern Chinese Altai: evidence from structural relationships and U–Pb geochronology. Lithos 314-315, 400–424.

Bryan, S., Ernst, R.E., 2008. Revised definition of Large Igneous Provinces (LIPs). Earth Sci. Rev. 86, 175–202.

Bryan, S.E., Peate, I.U., Peate, D.W., Self, S., Jerram, D.A., Mawby, M.R., Marsh, J.S. (Goonie), Miller, J.A., 2010. The largest volcanic eruptions on Earth. Earth Sci. Rev. 102 (3–4), 207–229.

Burke, K., Dewey, D.F., 1973. Plume generated triple junctions: key indicators in applying plate tectonics to old rocks. J. Geol. 81 (4), 406–433.

Cai, K., Sun, M., Yuan, C., Long, X., Xiao, W., 2011. Geological framework and Paleozoic tectonic history of the Chinese Altai, NW China: a review. Russ. Geol. Geophys. 52 (12), 1619–1633.

Campbell, I.H., 2001. Identification of ancient mantle plumes. In: Ernst, R.E., Buchan, K.L. (Eds.), Mantle Plumes: Their Identification through Times. Geological Society of America, Special Paper Vol. 352, pp. 5–21.

Carlson, R.W., 1991. Physical and chemical evidence on the cause and source characteristics of flood basalt volcanism. Aust. J. Earth Sci. 38, 525–544.

Chen, M., Niu, F., Liu, Q., Tromp, J., 2015. Mantle-driven uplift of Hangai Dome: new seismic constraints from adjoint tomography. Geophys. Res. Lett. 42, 6967–6974.

Chen, H., Xiau, Q.-K., Ingrin, J., Deloule, E., Bi, Y., 2017. Heterogeneous source components of intraplate basalts from NE China induced by the ongoing Pacific slab subduction. Earth Planet. Sci. Lett. 459, 208–220.

Condie, K.C., 1985. Plate Tectonics and Crustal Evolution. Pergamon Press, New York 305 p.

Condie, K.C., 2001. Mantle Plumes and their Record in Earth History. Cambridge University Press, Oxford. UK 306 p.

Cox, K.G., MacDonald, R., Hornung, G., 1967. Geochemical and petrological provinces in the Karoo basalts of southern Africa. Am. Mineral. 52, 1451–1474.

Cui, X., Sun, M., Zhao, G., Yao, J., Zhang, Y., Han, Y., Dai, L., 2020. A Devonian arc–back-arc basin system in the southern Chinese Altai: constraints from geochemical and Sr-Nd-Pb isotopic data for meta-basaltic rocks. Lithos 366–367, 1–15.

Devyatkin, E.V., 1974. Structures and formation complexes of the Cenozoic activation stage. In: Yanshin, A.L. (Ed.), Tectonics of the Mongolian People's Republic. Nauka Publishing House, Moscow, pp. 182–195 (in Russian).

Dobretsov, N.L., 2010. Distinctive petrological, geochemical, and geodynamic features of subduction-related magmatism. Petrology 18 (1), 84–106.

Dobretsov, N.L., 2011. Early Paleozoic tectonics and geodynamics of Central Asia: the role of mantle plumes. Russ. Geol. Geophys. 52 (12), 1539–1552.

Dobretsov, N.L., Buslov, M.M., Vernikovsky, V.A., 2003. Neoproterosoic to early Ordovician evolution of the Paleo-Asian Ocean: implications to the Break-up of Rodinia. Gondwana Res. 6 (2), 143–159.

Ernst, R.E., 2014. Large Igneous Provinces. Cambridge University Press 653 p.

Ernst, R.E., Buchan, K.L., Campbell, I.H., 2005. Frontiers in large igneous province research. Lithos 79, 271–297.

Ernst, R.E., Rodygin, S.A., Grinev, O.M., 2020. Age Correlation of Large Igneous Provinces with Devonian biotic crises. Glob. Planet. Chang. 185, 103097.

Ewart, A., Milner, S.C., Armstrong, R.A., Duncan, A.R., 1998. Etendeka volcanism of the Goboboseb Mountains and Messum Igneous Complex, Namibia. Part I: geochemical evidence of Early Cretaceous Tristan plume melts and the role of crustal contamination in the Paraná Etendeka CFB. J. Petrol. 39, 191–225.

Ewart, A., Marsh, J.S., Milner, S.C., Duncan, A.R., Kamber, B.S., Armstrong, R.A., 2004a. Petrology and geochemistry of early cretaceous bimodal continental flood volcanism of the NW Etendeka, Namibia: Part 1. Introduction, mafic lavas and reevaluation of mantle source components. J. Petrol. 45, 59–105.

Ewart, A., Marsh, J.S., Milner, S.C., Duncan, A.R., Kamber, B.S., Armstrong, R.A., 2004b. Petrology and geochemistry of early cretaceous bimodal continental flood volcanism of the NW Etendeka, Namibia: Part 2. Characteristics and petrogenesis of the high-Ti Latite and high-Ti and low-Ti voluminous quartz Latite Eruptives. J. Petrol. 45, 107–138.

Faure, G., 1986. Principles of Isotope Geology. John Wiley and Sons, New York 589 p.

Fedoseev, G.S., 2008. The role of mafic magmatism in age specification of Devonian continental trough deposits: evidence from the Minusa Basin, western Sibera, Russia. Bull. Geosci. 83 (4), 473–480.

Fedoseev, G.S., Ratanov, L.S., Travin, A.V., 2003. ^{40}Ar/^{39}Ar dating of sill complexes and volcanics of the Minusinsk intermontane depression (West Siberia). In: Kozakov, I.K., Kotov, A.B. (Eds.), Isotope Geochronology in Solving Problems of Geodynamics and Ore Genesis. Information Culture Center Publishing House, Saint Petersburg, pp. 518–521 (in Russian).

Gavrilova, S.P., Luvsandanzan, B., 1983. Devonian magmatism. In: Luchitsky, I.V. (Ed.), Continental Volcanism of Mongolia. Nauka Publishing House, Moscow, pp. 6–60 (in Russian).

Gordienko, I.V., 2006. Geodynamic evolution of late Baikalides and Paleozoids in the folded periphery of the Siberian craton. Russ. Geol. Geophys. 48 (1), 51–67.

Gradstein, F.M., Ogg, J.G., Schmitz, M.D., Ogg, G.M., 2012. The Geologic Time Scale 2012. The Geologic Time Scale. Published by Elsevier, Amsterdam https://doi.org/10.1016/C2011-1-08249-8 1176 p.

Gradstein, F., Ogg, J.G., Schmitz, M.D., Ogg, G.M. (Eds.), 2020. Geological Time-Scale 2020. Elsevier (in press).

Grinev, O.M., 1990. Evolution of Alkaline Gabbroid Magmatism of the Kuznetsk Alatau. Ph. D. dissertation abstract. Publishing House of Tomsk State University, Tomsk 18 p. (in Russian).

Grinev, O.M., 2007. Rift Systems of Siberia: Methodology of Investigations, Morphotectonics, Minerageny. Scientific & Technical Translations Publishing House, Tomsk 434 p. (in Russian).

Grinev, O.M., Vorontsov, A.A., Bogorodov, A.A., Adylbaev, R.R., Perfilova, O.Y., Grinev, R.O., 2019. Morphotectonics and the evolution of plum-riftogenic magmatism of Goryachegorsk volcanic plateau (Kuznetskiy Alatau). In: Ernst, R.E., Vrublevsky, V.V., Gladkochub, D.P., Gertner, I.F., Dobretsov, N.L., Izokh, A.E., Krasnova, T.S., Kruk, N.N., Kuzmin, M.I., Tishin, P.A., Tsygankov, A.A., Chernyshov, A.I. (Eds.), Large Igneous Provinces Through Earth History: Mantle Plumes, Supercontinents, Climate Change, Metallogeny and Oil-Gas, Planetary Analogues. CSTI Publishing house, Tomsk, pp. 43–44.

Hanyu, T., Tatsumi, Y., Nakai, S., Chang, Q., Miyazaki, T., Sato, K., Tani, K., 2006. Contribution of slab melting and slab dehydration to magmatism in the NE Japan arc for the last 25 Myr: constraints from geochemistry. Geochem. Geophys. Geosyst. 7 (8), 1–29.

Hawkesworth, C.J., Hergt, J.M., Ellam, R.M., McDermott, F., 1991. Element fluxes associated with subduction related magmatism. Philos. Trans. R. Soc. Lond. Ser. A 335, 393–405.

Hawkesworth, C.J., Gallagher, K., Hergt, J.M., McDermott, F., 1993. Mantle and slab contributions in arc magmas. Annu. Rev. Earth Planet. Sci. 21, 175–204.

Hawkesworth, C.J., Gallagher, K., Kirstein, L., Mantovani, M.S.M., Peate, D.W., Turner, S.P., 2000. Tectonic controls on magmatism associated with continental break-up: an example from the Paraná-Etendeka Province. Earth Planet. Sci. Lett. 179 (2), 335–349.

Hoang, N., Uto, K., 2003. Geochemistry of Cenozoic basalts in the Fukuoka district (northern Kyushu, Japan): implications for asthenosphere and lithospheric mantle interaction. Chem. Geol. 198 (3–4), 249–268.

Humphreys, E.R., Niu, Y., 2009. On the composition of ocean island basalts (OIB): the effects of lithospheric thickness variation and mantle metasomatism. Lithos 112, 118–136.

Ivanov, A.V., He, H.-Y., Yan, L.-K., Ryabov, V.V., Shevko, A.Y., Palesskii, S.V., Nikolaeva, I.V., 2013. Siberian Traps large igneous province: evidence for two flood basalt pulses around the Permo-Triassic boundary and in the Middle Triassic, and contemporaneous granitic magmatism. Earth Sci. Rev. 122, 58–76.

Izokh, A.E., Polyakov, G.V., Shelepaev, R.A., Vrublevskii, V.V., Egorova, V.V., Rudnev, S.N., Lavrenchuk, A.V., Borodina, E.V., Oyunchimeg, T., 2008. Early Paleozoic Large Igneous Province of the Central Asia Mobile Belt. Published on Large Igneous Provinces Commission. May 2008 LIP of the Month. http://www.largeigneousprovinces.org.

Izokh, A.E., Vishnevskii, A.V., Polyakov, G.V., Shelepaev, R.A., 2011. Age of picrite and picrodolerite magmatism in western Mongolia. Russ. Geol. Geophys. 52 (1), 7–23 (in Russian).

Jahn, B.-M., Wu, F., Chen, B., 2000. Granitoids of the Central Asian Orogenic Belt and continental growth in the Phanerozoic. Trans. R. Soc. Edinb. Earth Sci. 91, 181–193.

Jourdan, F., Bertrand, H., Sharer, U., Blicherrt-Toft, J., Féraud, G., Kampunzu, A., 2007. Major-trace element and Sr-Nd-Hf-Pb isotope compositions of the Karoo large igneous province in Botswana-Zimbabwe. J. Petrol. 48, 1043–1077.

Kelemen, P.B., Hanghøj, K., Greene, A.R., 2003. One view of the geochemistry of subduction-related magmatic arcs, with an emphasis on primitive andesite and lower crust. In: Holland, H.D., Turekian, K.K., Rudnick, R.L. (Eds.), Treatise on Geochemistry, The Crust. vol. 3. Elsevier Ltd, Oxford, pp. 594–649.

Khomichev, V.L., Smagin, A.N., Chunikhina, L.E., 2001. The Standard of the Imir Volcanic Complex (East Sayan). SNIIGGiMS Publishing House, Novosibirsk 208 p. (in Russian).

Kieffer, B., Arndt, N., Lapierre, H., Bastien, F., Bosch, D., Pecher, A., Yirgu, G., Ayalew, D., Weise, D., Jerram, D.A., Keller, F., Meugniot, C., 2004. Flood and shield basalts from Ethiopia: magmas from the African superswell. J. Petrol. 45, 793–834.

Kosorukov, A.P., Parnachev, V.P., 1994. Geological structure and stratigraphy of the volcanic-sedimentary series of the western part of the Kopievsky dome of the Chebakovo-Balakhtinsky depression (Minusinsk depression). In: Rodygin, V.M., Podobina, S.A. (Eds.), Problems of Geology of Siberia 1. TGU publishing house, Tomsk, pp. 27–36 (in Russian).

Kovalenko, V.I., Tsaryova, G.M., Goreglyad, A.V., Yarmolyuk, V.V., Arakelyants, M.M., 1989. Geology and petrography of peralkaline rare-metal granitoids of the Khaldzan-Buregtei massif (Mongolian Altai). Izv. Acad. Sci. USSR 9, 25–35 (in Russian).

Kovalenko, V.I., Yarmolyuk, V.V., Sal'nikova, E.B., Kartashov, P.M., Kovach, V.P., Kozakov, I.K., Kozlovskii, A.M., Kotov, A.B., Ponomarchuk, V.A., Listratova, E.N., Yakovleva, S.Z., 2004a. The Khaldzan-Buregtei massif of peralkaline rare-metal igneous rocks: structure, geochronology, and geodynamic setting in the Caledonides of Western Mongolia. Petrology 12 (5), 412–436.

Kovalenko, V.I., Yarmolyuk, V.V., Kozlovskii, A.M., Kovach, V.P., Sal'nikova, E.B., Kotov, A.B., Khanchuk, A.I., 2004b. Multiple magma sources for the peralkaline granitioids and related rocks of the Khaldzan Buregte group of massifs, Western Mongolia: isotopic (neodymium, strontium, and oxygen) and geochemical data. Petrology 12 (6), 497–518.

Krasnov, V.I., Ratanov, L.S., 1974. About the stratotypes of the Matarak and Shunet suite in the North Minusinsk depression. In: Sukhov, S.V., Krasnov, V.I. (Eds.), Materials on

Regional Geology. SNIIGGiMS Publishing House, 173, Novosibirsk, pp. 82–89 (in Russian).

Kravchinsky, V.A., 2012. Paleozoic large igneous provinces of Northern Eurasia: correlation with mass extinction events. Glob. Planet. Chang. 86-87, 31–36.

Kröner, A., Kovach, V., Belousova, E., Hegner, E., Armstrong, R., Dolgopolova, A., Seltmann, R., Alexeiev, D.V., Hoffmann, J.E., Wongj, J., Suni, M., Cai, K., Wang, T., Tong, Y., Wilde, S.A., Degtyarev, K.E., Rytsk, E., 2014. Reassessment of continental growth during the accretionary history of the Central Asian Orogenic Belt. Gondwana Res. 25, 103–125.

Kröner, A., Kovach, V., Alexeiev, D., Wang, K.L., Wong, J., Degtyarev, K., Kozakov, I., 2017. No excessive crustal growth in the Central Asian Orogenic Belt: further evidence from field relationships and isotopic data. Gondwana Res. 50, 135–166.

Kruk, N.N., 2015. Continental crust of Gorny Altai: stages of formation and evolution; indicative role of granitoids. Russ. Geol. Geophys. 56, 1097–1113.

Kruk, N.N., Babin, G.A., Kruk, E.A., Rudnev, S.N., Kuybida, M.L., 2008. Petrology of volcanic and plutonic rocks of the Uimeno-Lebedsky area, Gorny Altai. Russian Petrology 16 (5), 548–568.

Kruk, N.N., Rudnev, S.N., Vladimirov, A.G., Shokalsky, S.P., Kovach, V.P., Serov, P.A., Volkova, N.I., 2011. Early-middle Paleozoic granitoids in Gorny Altai, Russia: Implications for continental crust history and magma sources. J. Asian Earth Sci. 42, 928–948.

Krupchatnikov, V.I., Vrublevskii, V.V., Kruk, N.N., 2018. Early Devonian volcanics of southeastern Gorny Altai: geochemistry, isotope (Sr, Nd, and O) composition, and petrogenesis (Aksai complex). Russ. Geol. Geophys 59 (8), 905–924.

Kuibida, M.L., Kruk, N.N., Shokal'skii, S.P., 2015. Subduction plagiogranites of Rudny Altai: Age and composition characteristics. Dokl. Akad. Sci. 464, 914–918 (in Russian).

Kuibida, M.L., Murzin, O.V., Kruk, N.N., Safonova, I.Y., Sun, M., Komiya, T., Wong, J., Aoki, S., Murzina, N.M., Nikolaeva, I., Semenova, D.V., Khlestov, M., Shelepaev, R.A., Kotler, P.D., Yakovlev, V.A., Naryzhnova, A.V., 2020. Whole-rock geochemistry and U-Pb ages of Devonian bimodal-type rhyolites from the Rudny Altai, Russia: petrogenesis and tectonic settings. Gondwana Res. 81, 312–338.

Kuzmin, M.I., Yarmolyuk, V.V., Kravchinsky, V.A., 2010. Phanerozoic hot spot traces and paleogeographic reconstructions of the Siberian continent based on interaction with the African large low shear velocity province. Earth Sci. Rev. 102, 29–59.

Kuznetsov, V.A., 1966. General characteristics of Tuva magmatism. In: Kudryavtsev, G.A., Kuznetsov, V.A. (Eds.), Geology of the USSR 29 (1). Nedra Publishing House, Moscow, pp. 249–255 (in Russian).

Lavrenchuk, A.V., Izokh, A.E., Polyakov, G.V., Metelkin, D.V., Mikhal'tsov, N.E., Travin, A.V., 2004. The Chernaya sopka teshenite-syenite complex of the Northwestern east sayans: an expression of early Devonian plume magmatism. Russ. Geol. Geophys. 45 (6), 618–634.

Le Bas, M.J., Le Maitre, R.W., Streckeisen, A., Zanettin, B., 1986. Chemical classification of volcanic rocks based on the Total Alkali-Silica Diagram. J. Petrol. 27, 745–750.

Le Maitre, R.W., Bateman, P., Dudek, A., Keller, J., Lameyer, J., Le Bas, M.J., Sabine, P.A., Schmid, R., Sørensen, H., Streckeisen, A., Woolley, A.R., Zanettin, B. (Eds.), 1997. Chapter B: Glossary of Terms. Classification of Igneous Rocks and Glossary of Terms. Recommendations of the International Union of Geological Sciences Subcommission on the Systematics of Igneous Rocks. Nedra Publishing House, Moscow, pp. 48–142 (in Russian).

Lee, M.J., Lee, J.I., Kwon, S.T., Choo, M.K., Jeong, K.S., Cho, J.H., Kim, S.R., 2011. Sr-Nd-Pb isotopic compositions of submarine alkali basalts recovered from the South Korea Plateau, East Sea. Geosci. J. 15 (2), 149–160.

Li, T. (Ed.), 2008. Atlas of Geological Maps of Central Asia and Adjacent Areas. Geological Publishing House, Beijing 8 Sheets, 1: 2500000.

Litvinovsky, B.A., Zanvilevich, A.N., Shadaev, M.G., Posokhov, V.F., Yarmolyuk, V.V., Nikiforov, A.V., 2005. Sources of material and genesis of granitic pegmatites of the Oshurkovskii alkaline monzonite massif, transbaikalia. Geochem. Int. 43 (12), 1149–1167.

Liu, Y., Li, W., Feng, Z., Wen, Q., Neubauer, F., Liang, C., 2017. A review of the Paleozoic tectonics in the eastern part of Central Asian Orogenic Belt. Gondwana Res. 43, 123–148.

Luchitsky, I.V., 1960. Volcanism and Tectonics of the Devonian Depressions of the Minusinsk Intermountain Trough. Academy of Sciences of the USSR Publishing House, Moscow 276 p. (in Russian).

Maitre (Ed.), Le, Streckeisen, A., Zanettin, B., Le Bas, M.J., Bonin, B., Bateman, P., Bellieni, G., Dudek, A., Efremova, S., Keller, J., Lameyre, J., Sabine, P.A., Schmid, R., Sørensen, H., Woolley, A.R., 2002. A Classification and Glossary of Terms: Recommendations of the International Union of Geological Sciences Subcommission on the Systematics of Igneous Rocks. Cambridge University Press, New York 236 p. http://www.cambridge.org/resources/052166215x http://www.cambridge.org/9780521662154>.

Makarenko, N.A., Kortusov, M.P., 1991. Petrology of the Gabbro-Syenite-Nepheline-Syenite Association of the Mariinsky Taiga. Tomsk University Publishing House, Tomsk 310 p. (in Russian).

Malkovets, V.G., Litasov, Y.D., Travin, A.V., Litasov, K.D., Taylor, L.A., 2003. Volcanic pipes as clues to upper mantle petrogenesis: mesozoic Ar-Ar dating of the Minusinsk basalts, South Siberia. Int. Geol. Rev. 45 (2), 133–142.

Markov, V.N., 1987. About the effusive nature of the bereshites of the western margin of the North Minusinsk depression. In: Kortusov, M.P. (Ed.), Alkaline and Moderately Alkaline Rocks of the Kuznetsk Alatau. Tomsk University Publishing House, Tomsk, pp. 92–96 (in Russian).

Marsh, J.S., Ewart, A., Milner, S.C., Duncan, A.N., Miller, R. McG, 2001. The Etendeka igneous province: magma types and their stratigraphic distribution with implications for the evolution of the Paraná-Etendeka flood basalt province. Bull. Volcanol. 62, 464–486.

Martynov, Yu., 1999. High-alumina basaltic volcanism of the Eastern Sikhote Alin: petrology and geodynamics. Petrology 7 (1), 58–79 (in Russian).

Miyashiro, A., 1974. Volcanic rock series in island arcs and active continental margins. Am. J. Sci. 274, 321–355.

Mordvinova, V.V., Treusov, A.V., Turutanov, E.Kh., 2015. Nature of the mantle plume under Hangai (Mongolia) based on seismic and gravimetric data. Dokl. Earth Sci. 460, 92–95.

Murzin, O.V., Gorshechnikov, V.I., Chekalin, V.M., Gusev, N.I., Bedarev, N.P., 2001. Geological Report to State Geological Map of the Russian Federation. Altai Series. Scale 1: 200,000. Sheet M-44-X and XI. Second ed. Sankt-Peterburgskaya Kartograficheskaya Fabrika, Saint Petersburg p. 304 (in Russian).

Nagibina, M.S., 1974. Structures and formation complexes of Mesozoic revival and activation. In: Yanshin, A.L. (Ed.), Tectonics of the Mongolian People's Republic. Nauka Publishing House, Moscow, pp. 165–178 (in Russian).

Neumann, E.-R., Svensene, H., Galerne, C.Y., Planke, S., 2011. Multistage evolution of dolerites in the Karoo Large Igneous Province, Central South Africa. J. Petrol. 52, 959–984.

Nozhkin, A.D., Smagin, A.N., 1979. The experience of the dismemberment and correlation of the Devonian volcanogenic formations of the northwestern part of the Agul depression using radiogeochemical data. In: Polyakov, G.V. (Ed.), Magmatic Complexes of Eastern Siberia. IGG of USSR Academy of Sciences Publishing House, Novosibirsk, pp. 72–95 (in Russian).

Ohapkin, N.A., 1961. Devonian travertines of the Kopievo region (Minusinsky intermountain trough). Russ. Geol. Geophys. 5, 80–82.

Parnachev, V.P., 2006. Devonian volcanism of the Altai-Sayan folded region (lateral variations in composition and geodynamic conditions of manifestation). In: Gordienko, I.V. (Ed.), Volcanism and Geodynamics. Buryat Scientific Center of the SB RAS Publishing House, Ulan-Ude, pp. 264–267 (in Russian).

Parnachev, V.P., Vyltsan, I.A., Makarenko, N.A., Bezhentsev, A.F., Smagin, A.N., Zaikov, V.V., Gutak, Y.N., Tatyanin, G.M., Chuvakin, V.S., Kuzovatov, N.I., 1996. Devonian Rift Formations in the South of Siberia. Tomsk State University Publishing House, Tomsk 239 p. (in Russian).

Pearce, J.A., 1982. Trace element characteristics of lavas from destructive plate boundaries. In: Thorpe, R.S. (Ed.), Andesites. John Wiley & Sons, New York, pp. 525–548.

Pearce, J.A., Peate, D.W., 1995. Tectonic implications of the composition of volcanic ARC magmas. Annu. Rev. Earth Planet. Sci. 23, 251–285.

Pearce, J.A., Harris, N.B., Tindle, A.G., 1984. Trace element discrimination diagrams for the tectonic interpretation of granitic rocks. J. Petrol. 25, 956–983.

Peate, D.W., 1997. The Paraná-Etendeka Province. AGU Geophys. Monogr. 100, 217–245.

Peate, D.W., Hawkesworth, C.I., Maritovani, M.S., 1992. Cemical stratigraphy of the Parana Lavas (South America): classificatiation of magma types and their spatial distribution. Bull. Volcanol. 55, 119–139.

Perfilova, O.Yu., Mikhailenko, V.V., Koptev, I.I., Sidoras, S.D., 1999. Koshkulak Standard of the Ordovician Volcanic-Plutonic Association (Kuznetsk Alatau). KNIIGIMS Publishing House, Krasnoyarsk 159 p. (in Russian).

Perfilova, O.Yu., Makhlaev, M.L., Sidoras, S.D., 2004. Ordovician volcanic-plutonic association in structures of the folded surrounding of the Minusa depression. Rus. Lit. 3, 137–152.

Pirajno, F., 2010. Intracontinental strike-slip faults, associated magmatism, mineral systems and mantle dynamics: examples from NW China and Altai-Sayan (Siberia). J. Geodyn. 50 (3–4), 325–346.

Polyakov, G.V., Dovgal, V.N., Teleshev, A.E., Fedoseev, G.S., Bognibov, V.I., 1972. Lateral variability of effusive-intrusive associations of zones of the Middle Paleozoic activation of the Caledonian-Baikal structures of the Altai-Sayan folded region. Dokl. Akad. Sci. USSR 203, 1374–1377 (in Russian).

Puffer, J.H., 2001. Contrasting HFSE contents of plume sourced and reactivated arc-sourced continental flood basalts. Geology 29, 675–678.

Rotarash, A.I., Samygin, S.G., Gredyushko, Y.A., Keyl'man, G.A., Mileyev, V.S., Perfil'yev, A.S., 1982. The Devonian active continental margin in the southwest Altai. Geotectonics 16, 31–41 (in Russian).

Rublev, A.G., Makhlaev, M.L., 1997. The age of the border is early-middle Devonian. Nat. Geol. 5, 22–25 (in Russian).

Rublev, A.G., Shergina, Yu.P., Shkorbatova, G.S., 1994. Devonian magmatism of the agul depression. Nat. Geol. 3, 42–48 (in Russian).

Rublev, A.G., Shergina, Yu.P., Berzon, E.I., 1999. The isotopic age of the Paleozoic volcanics of the Krasnoyarsk outcrop and the problem of stratigraphy of the Byskar series. Nat. Geol. 3, 47–54 (in Russian).

Rudnev, S.N., 2013. Early Paleozoic Granitoid Magmatism of the Altai-Sayan Folded Region and the Lake Zone of Western Mongolia. Publishing House of the SB RAS, Novosibirsk 300 p. (in Russian).

Rudnev, S.N., Kruk, N.N., Gusev, A.I., Shokalsky, S.P., Kotov, A.B., Salnikova, E.B., Levchenko, O.A., 2001. The nature of the Altai-Minusinsk volcanic-plutonic belt (according to geochemical and U-Pb geochronological studies of granitoids). Materials of a scientific and practical conference: actual problems of geology and mineralogeny of the South of Siberia. Novosibirsk 231–242 (in Russian).

Rudnev, S.N., Izokh, A.E., Kovach, V.P., Shelepaev, R.A., Terent'eva, L.B., 2009. Age, composition, sources, and geodynamic environments of the origin of granitoids in the northern part of the Ozernaya Zone, Western Mongolia: growth mechanisms of the Paleozoic continental crust. Petrology 17 (5), 439–475.

Rudnev, S.N., Kovach, V.P., Ponomarchuk, V.A., 2013. Vendian-early Cambrian island-arc plagiogranitoid magmatism in the Altai-Sayan fold belt and in the Lake Zone of western Mongolia (geochronological, geochemical, and isotope data). Russ. Geol. Geophys. 54 (10), 1272–1287.

Rudnick, R.L., Gao, S., 2003. Composition of the continental crust. In: Holland, H.D., Turekian, K.K., Rudnick, R.L. (Eds.), Treatise on Geochemistry, The Crust. Vol. 3. Elsevier Ltd, Oxford, pp. 1–56.

Ryerson, F.J., Watson, E.B., 1987. Rutile saturation in magmas: implications for Ti – Nb – Ta depletion in island-arc basalts. Earth Planet. Sci. Lett. 86, 225–239.

Safonova, I.Yu., Santosh, M., 2014. Accretionary complexes in the Asia-Pacific region: tracing archives of ocean plate stratigraphy and tracking mantle plumes. Gondwana Res. 25, 126–158.

Sakuyama, T., Tian, W., Kimura, J.-I., Fukao, Y., Hirahara, Y., Takahashi, T., Senda, R., Chang, Q., Miyazaki, T., Obayashi, M., Kawabata, H., Tatsumi, Y., 2013. Melting of dehydrated oceanic crust from the stagnant slab and of the hydrated mantle transition zone: constraints from Cenozoic alkaline basalts in Eastern China. Chem. Geol. 359 (14), 32–48.

Saunders, A.D., Storey, M., Kent, R.W., Norry, M.J., 1992. Consequences of plume–lithosphere interactions. In: Storey, B.C., Alabaster, T., Pankhurst, R.J. (Eds.), Magmatism and the Causes of Continental Breakup. Geological Society of London Special Publication Vol. 68, pp. 41–60 London.

Scambelluri, M., Philippot, P., 2001. Deep fluids in subduction zones. Lithos 55, 213–227.

Scherba, G.N., D'yachkov, B.A., Stuchevsky, N.I., Nakhtigal, G.P., Antonenko, A.N., Lubetsky, V.N., 1998. The Great Altai (geology and metallogeny). Book 1. Almaty, Gylym 304 p. (in Russian).

Schneider, E.A., Zubkus, B.P., 1962. Stratigraphy of the lower and Middle Devonian deposits of the North Minusinsk and Sydo-Yerbinsk depressions. In: Aladyshkin, A.S. (Ed.), Materials on the geology and minerals of the Krasnoyarsk Territory. Vol. 3. Krasnoyarsk Publishing House, Krasnoyarsk, pp. 41–56 (in Russian).

Sengör, A.M.C., Natal'in, B.A., Burtman, V.S., 1993. Evolution of the Altaid tectonic collage and Paleozoic crustal growth in Eurasia. Nature 364, 299–307.

Sennikov, N.V., Grazianova, R.T., Sobolev, E.S., Klets, T.V., 1995. On the origin and age of the Aramchak formation of the Lower Devonian in the North Minusinsk depression. Russ. Geol. Geophys. 36 (3), 15–24.

Shokalsky, S.P., Babin, G.A., Vladimirov, A.G., 2000. Correlation of Magmatic and Metamorphic Complexes in the Western Part of the Altai-Sayan Folded Region. Geo Publishing House, Novosibirsk 187 p. (in Russian).

Sugorakova, A.M., Nikiforov, A.V., Bolonin, A.V., 2009. Devonian magmatism of the Tuvinian Trough. Large Igneous Provinces of Asia, Mantle Plumes and Metallogeny: Abstracts of the International Symposium. Sipprint, Novosibirsk, pp. 353–355.

Sun, S.S., McDonough, W.F., 1989. Chemical and isotopic systematics of oceanic basalts: implications for mantle composition and processes. In: Saunders, A.D., Norry, M.J. (Eds.), Magmatism in the Ocean Basins. Geological Society, Special Publications Vol. 42, pp. 313–346 London.

Tatsumi, Y., Eggins, S.M., 1995. Subduction Zone Magmatism. Blackwell Science, Oxford 211 p.

Theodorovich, G.I., Polonskaya, B.Ya., 1958. Stratigraphy, Petrography and Facies of the Devonian of the Minusinsky and Nazarovskaya Depressions. Publishing House of the USSR Academy of Sciences, Moscow 232 p. (in Russian).

Thompson, R.N., Morrison, M.A., Hendry, G.L., Parry, S.J., 1984. An assessment of the relative roles of a crust and mantle in magma genesis: an elemental approach. Philos. Trans. R. Soc. Lond. Ser. A 310, 549–590.

Tikunov, Yu.V., 1995. Geochemistry of Devonian basalt-andesitic volcanism in the western part of Gorny Altai. Russ. Geol. Geophys. 36 (2), 61–69.

Till, C.B., Grove, T.L., Withers, A.C., 2011. The beginnings of hydrous mantle wedge melting. Contrib. Mineral. Petrol. 163, 669–688.

Uvarov, A.N., Uvarova, N.M., 2008. Petrotype of the Goryachegorsk Alkaline-Gabbroid Complex (Kuznetsk Alatau). SNIIGGiMS Publishing House, Novosibirsk 191 p. (in Russian).

Uvarov, A.N., Uvarova, N.M., 2009. Petrotype of the Sokolinogorsk Trachybasalt-Epileocytophonolite Complex. SNIIGGiMS Publishing House, Novosibirsk 108 p. (in Russian).

Vladimirov, A.G., Gibsher, A.S., Izokh, A.E., Rudnev, S.N., 1999. Early Paleozoic Granitoid Batholiths of Central Asia: abundance, sources, and geodynamic formation conditions. Dokl. Earth Sci. 369 (9), 1268–1272.

Vladimirov, A.G., Kruk, N.N., Rudnev, S.N., Khromykh, S.V., 2003. Geodynamics and granitoids magmatism of collision orogens. Russ. Geol. Geophys. 44 (12), 1321–1338.

Vorontsov, A.A., 1993. Petrochemical characteristics of Devonian alkaline-alkaline magmatism of northwestern Mongolia. Russ. Geol. Geophys. 34 (8), 117–124.

Vorontsov, A.A., Sandimirov, I.V., 2010. The devonian magmatism in the Kropotkin Ridge (East Sayan) and sources of basites: geological, geochemical, and Sr-Nd isotope data. Russ. Geol. Geophys. 51 (8), 833–845.

Vorontsov, A.A., Yarmolyuk, V.V., Ivanov, V.G., Sandimirova, G.P., Pakholchenko, Y.A., 1997. Sources of basaltic melts for Devonian rift bimodal igneous associations of central Asia: evidence from trace element and strontium isotopic data on basic rocks from northeastern Mongolia. Petrology 5 (3), 208–222.

Vorontsov, A.A., Andryushchenko, S.V., Pakhol'chenko, Yu.A., Fedoseev, G.S., 2011. Sources of Devonian Magmatism in the Minusa Trough based on geochemical and Sr-Nd isotopic characteristics of basites. Dokl. Earth Sci. 441 (2), 1649–1655.

Vorontsov, A.A., Fedoseev, G.S., Travin, A.V., Perfilova, O.Yu., 2013a. Devonian volcanism of the Minusinsk basin: activity stages and relationship to downwarping of the continental lithosphere (based on ^{40}Ar-^{39}Ar geochronological studies). Dokl. Earth Sci. 448 (1), 25–30.

Vorontsov, A.A., Andryushchenko, S.V., Fedoseev, G.S., 2013b. Devonian volcanism in the Minusa basin in the Altai-Sayan area: geological, geochemical, and Sr–Nd isotopic characteristics of rocks. Russ. Geol. Geophys. 54 (9), 1001–1025.

Vorontsov, A.A., Gazizova, T.F., Yarmolyuk, V.V., Fedoseev, G.S., Travin, A.V., Perfilova, O.Y., Posokhov, V.F., 2015. Differentiated volcanic association of the Minusa trough: mechanisms of formation and sources of melts, as examplified by Batenevo rise. Petrology 23 (4), 353–375.

Vorontsov, A.A., Perfilova, O.Y., Kruk, N.N., 2018. Geodynamic setting, structure, and composition of continuous trachybasalt-trachiandesite-rhyolite series in the northe of Altai-Sayan area: the role of crust-mantle interaction in continental magma formation. Russ. Geol. Geophys. 59 (12), 1640–1659.

Vrublevsky, V.V., Grinev, O.M., Izokh, A.E., Travin, A.V., 2016. Geochemistry, isotopic triad (Nd-Sr-O) and ^{40}Ar-^{39}Ar age of Paleozoic alkaline mafic intrusions of the Kuznetsk Alatau (by the example of the Belaya Gora pluton). Russ. Geol. Geophys. 57 (3), 464–472.

Wang, T., Tong, Y., Li, S., Zhang, J.-J., Shi, X.-J., Li, J.-Y., Han, Bao-F, Hong, D.-W., 2010. Spatial and temporal variations of granitoids in the Altay orogen and their implications for tectonic setting and crustal growth: perspectives from Chinese Altay. Acta Petrol. Mineral. 29, 595–618 (in Chinese with English abstract).

Wang, Y., Zhao, Z.F., Zheng, Y.F., Zhang, J.J., 2011. Geochemical constraints on the nature of mantle source for Cenozoic continental basalts in east-Central China. Lithos 125 (3–4), 940–955.

Wang, Z.W., Pei, F.P., Xu, W.L., Cao, H.H., Wang, Z.J., Zhang, J., 2016. Tectonic evolution of the eastern Central Asian Orogenic Belt: evidence from zircon U–Pb–Hf isotopes and geochemistry of early Paleozoic rocks in Yanbian region, NE China. Gondwana Res. 38, 334–350.

Wilson, M., 1989. Igneous Petrogenesis. Unwin Hyman, London 464 p.

Windley, B.F., Alexeiev, D.V., Xiao, W., Kröner, A., Badarch, G., 2007. Tectonic models for accretion of the Central Asian Orogenic belt. J. Geol. Soc. Lond. 164, 31–47.

Wood, D.A., 1980. The application of a Th–Hf–Ta diagram to problems of tectonomagmatic classification and to establishing the nature of crustal contamination of basaltic lavas of British Tertialy volcanic province. Earth Planet. Sci. Lett. 50, 11–30.

Wooden, J.L., Czamanske, G.D., Fedorenko, V.A., Arndt, N.T., Chauvel, C., Bouse, R.M., King, Bi-Shia W., Knight, R.J., Seim, D.F., 1993. Isotopic and trace-element constraints on mantle and crustal contributions to Siberian continental flood basalts, Noril'sk area, Siberia. Geochim. Cosmochim. Acta 57, 3677–3704.

Xia, L.Q., 2014. The geochemical criteria to distinguish continental basalts from arc related ones. Earth Sci. Rev. 139, 195–212.

Xia, L.Q., Li, X.M., 2019. Basalt geochemistry as a diagnostic indicator of tectonic setting. Gondwana Res. 65, 43–67.

Xia, L.Q., Xia, Z.C., Xu, X.Y., Li, X.M., Ma, Z.P., 2008. Relative contributions of crust and mantle to the generation of the Tianshan Carboniferous rift-related basic lavas, northwestern China. J. Asian Earth Sci. 31, 357–378.

Xiao, W.J., Huang, B.C., Han, C.M., Sun, S., Li, J.L., 2010. A review of the western part of the Altaids. Gondwana Res. 18, 253–273.

Xu, Y.-G., He, B., Chung, S.-L., Menzis, M.A., Frey, F.A., 2004. Geologic, geochemical, and geophysical consequences of plume involvement in the Emeishan flood-basalt province. Geology 32, 917–920.

Yarmolyuk, V.V., Kovalenko, V.I., 1991. Rift Magmatism of Active Continental Margins and its Ore Potential. Nauka Publishing House, Moscow 263 p. (in Russian).

Yarmolyuk, V.V., Kovalenko, V.I., 2003. Deep geodynamics and mantle plumes: role in formation of the Central-Asian folded belt. Petrology 1 (6), 504–531.

Yarmolyuk, V.V., Vorontsov, A.A., 1993. Devonian volcanism of the eastern framing of Mongolian Altai and its structural control. Geotektonika 4, 76–86 (in Russian).

Yarmolyuk, V.V., Kovalenko, V.I., Ivanov, V.G., 1996. The intraplate Late Mesozoic–Cenozoic volcanic province in Central East Asia as a projection of the mantle hot field. Geotectonics 29 (5), 395–421.

Yarmolyuk, V.V., Ivanov, V.G., Kovalenko, V.I., 1998. Sources of intraplate magmatism in Western Transbaikalia in the Late Mesozoic – Cenozoic (based on geochemical and isotope data). Petrology 6 (2), 115–138 (in Russian).

Yarmolyuk, V.V., Kovalenko, V.I., Kuz'min, M.I., 2000. North Asian Superplume activity in the Phanerozoic: magmatism and geodynamics. Geotectonics 5, 343–366.

Yarmolyuk, V.V., Kovalenko, V.I., Kovach, V.P., Rytsk, E.Yu., Kozakov, I.K., Kotov, A.B., Sal'nikova, E.B., 2006. Early Stages of the Paleoasian Ocean formation: results of geochronological, isotopic, and geochemical investigations of Late Riphean and Vendian-Cambrian complexes in the Central Asian fold belt. Dokl. Earth Sci. 411 (8), 1184–1189.

Yarmolyuk, V.V., Kovalenko, V.I., Kozlovsky, A.M., Kovach, V.P., Sal'nikova, E.B., Kovalenko, D.V., Kotov, A.B., Kudryashova, E.A., Lebedev, V.I., Eenzhin, G., 2008. Crust-forming processes in the Hercynides of the Central Asian foldbelt. Petrology 16 (7), 679–709.

Yarmolyuk, V.V., Kudryashova, E.A., Kozlovsky, A.M., Savatenkov, V.M., 2011a. Late Cenozoic volcanic province in Central and East Asia. Petrology 19 (4), 327–347.

Yarmolyuk, V.V., Kovach, V.P., Kovalenko, V.I., Sal'nikova, E.B., Kozlovsky, A.M., Kotov, A.B., Yakovleva, S.Z., Fedoseenko, A.M., 2011b. Composition, sources, and mechanism of continental crust growth in the Lake Zone of the Central Asian Caledonides: I. Geological and geochronological data. Petrology 19 (1), 55–78.

Yarmolyuk, V.V., Kuz'min, M.I., Vorontsov, A.A., 2013. Convergent boundaries of the West Pacific type and their role in the formation of the Central Asian fold belt. Russ. Geol. Geophys. 54 (12), 1427–1441.

Yarmolyuk, V.V., Kuz'min, M.I., Ernst, R.E., 2014. Intraplate geodynamics and magmatism in the evolution of the Central Asian Orogenic Belt. J. Asian Earth Sci. 93, 158–179.

Yarmolyuk, V.V., Kudryashova, E.A., Kozlovsky, A.M., Lebedev, V.A., Savatenkov, V.M., 2015. Late Mesozoic–Cenozoic intraplate magmatism in Central Asia and its relation with mantle diapirism: evidence from the South Khangai volcanic region, Mongolia. J. Asian Earth Sci. 111 (1), 604–623.

Yarmolyuk, V.V., Kozlovsky, A.M., Savatenkov, V.M., Kovach, V.P., Kozakov, I.K., Kotov, A.B., Lebedev, V.I., Eenjin, G., 2016. Composition, sources, and geodynamic nature of giant batholiths in Central Asia: evidence from the geochemistry and Nd isotopic characteristics of granitoids in the Khangai zonal magmatic area. Petrology 24 (5), 433–461.

Yarmolyuk, V.V., Nikiforov, A.V., Kozlovsky, A.M., Kudryashova, E.A., 2019. Late Mesozoic East Asian Magmatic Province: structure, magmatic signature, formation conditions. Geotectonics 53 (4), 500–516.

Yashina, R.M., 1982. Alkaline Magmatism of Folded-Block Areas (on the Example of the Southern Frame of the Siberian Platform). Nauka Publishing House, Moscow 276 p. (in Russian).

Yoshida, T., Kimura, J.-I., Yamada, Y., Acocella, V., Sato, H., Zhao, D., Nakajima, J., Hasegawa, A., Okada, T., Honda, T., Ishikawa, M., Prima, O.D.A., Kudo, T., Shibazaki, B., Tanaka, A.,

Imaizumi, T., 2014. Evolution of late Cenozoic magmatism and the crust-mantle structure in the NE Japan Arc. In: Gómez-Tuena, A., Straub, S.M., Zellmer, G.F. (Eds.), Orogenic Andesites and Crustal Growth. Geological Society of London, Special Publications Vol. 385, pp. 335–387.

Zakharova, T.V., Ananiev, A.R., 1990. On the stratigraphic position of the Byskarian series of the Devonian Minusinsk trough. Bull. Mosc. Soc. Nat. Testers. Dep. Geol. 65 (2), 44–50 (in Russian).

Zhao, J.-X., Malcolm, M.T., Korsch, R.J., 1994. Characterisation of a plume-related *c.* 800 Ma magmatic event and its implications for basin formation in Central-Southern Australia. Earth Planet. Sci. Lett. 121, 349–367.

Zhao, G., Wang, Y., Huang, B., Dong, Y., Li, S., Zhang, G., Yu, S., 2018. Geological reconstructions of the East Asian blocks: from the breaking of Rodinia to the assembly of Pangea. Earth Sci. Rev. 186, 262–286.

Zindler, A., Hart, S., 1986. Chemical geodynamics. Annu. Rev. Earth Planet. Sci. 14, 493–571.

Zonenshain, L.P., Kuzmin, M.I., Natapov, L.M., 1991. Geology of the USSR: A Plate-Tectonic Synthesis. American geophysical Union, Washington 442 p.

Zubkov, V.S., Pakhol'chenko, Yu.A., Sandimirova, G.P., Mamitko, V.R., Plyusnin, G.S., 1986. Rubidium-strontium age and genesis of alkaline olivine basalts of the Minusinsk depression system. Dokl. Akad. Sci. USSR 290 (4), 960–963 (in Russian).